HHS Public Access

Author manuscript

*Brain Behav Immun*. Author manuscript; available in PMC 2021 August 01.

Published in final edited form as:

*Brain Behav Immun*. 2020 August ; 88: 363–380. doi:10.1016/j.bbi.2020.03.034.

# Electronic cigarette exposure disrupts blood-brain barrier integrity and promotes neuroinflammation

**Nathan A. Heldt**[1,2], **Alecia Seliga**[1], **Malika Winfield**[1], **Sachin Gajghate**[1], **Nancy Reichenbach**[1], **Xiang Yu**[3], **Slava Rom**[1,2], **Amogha Tenneti**[1], **Dana May**[1], **Brian D. Gregory**[3], **Yuri Persidsky**[1,2]

[1]Department of Pathology and Laboratory Medicine, Lewis Katz School of Medicine, Temple University, Philadelphia, PA, USA

[2]Center for Substance Abuse Research, Lewis Katz School of Medicine, Temple University, Philadelphia, PA, USA

[3]Department of Biology, University of Pennsylvania, Philadelphia, PA, USA

## Abstract

Electronic cigarette (e-cigarette) use has grown substantially since inception, particularly among adolescents and combustible tobacco users. Several cigarette smoke constituents with known neurovascular effect are present in e-cigarette liquids or formed during the vapor generation. The present study establishes inhaled models of cigarette and e-cigarette use with normalized nicotine delivery, then characterizes the impact on blood-brain barrier function. Sequencing of microvessel RNA following exposure revealed downregulation of several genes with critical roles in BBB function. Reduced protein expression of Occludin and Glut1 is also observed at the tight junction in all groups following exposure. Pro-inflammatory changes in leukocyte-endothelial cell interaction are also noted, and mice exposed to nicotine-free e-cigarettes have impaired novel object recognition performance. On this basis, it is concluded that long term e-cigarette use may adversely impact neurovascular health. The observed effects are noted to be partly independent of nicotine content and nicotine may even serve to moderate the effects of non-nicotinic components on the blood-brain barrier.

## Graphical Abstract

Corresponding Authors: Nathan Heldt, nathan.heldt@temple.edu; Yuri Persidsky, yuri.persidsky@tuhs.temple.edu, Department of Pathology and Laboratory Medicine, Lewis Katz School of Medicine, Temple University, 3500 N. Broad Street, MERB 880A, Philadelphia, PA 19140, T: (215) 707-2543.



The authors declare no competing financial interests.

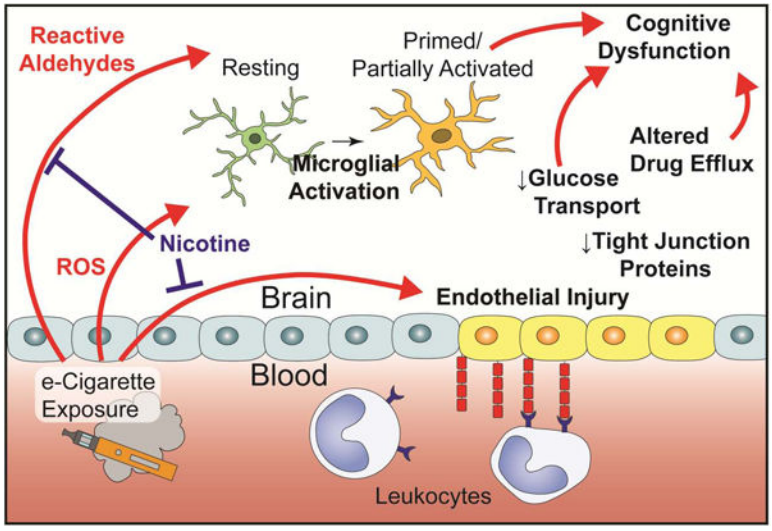


**Keywords**

e-cigarette; vaping; nicotine; blood-brain barrier; neuroinflammation

## 1. Introduction

The increasing popularity of electronic cigarettes (e-cigarettes, ‘vaping’) over the last decade has generated several urgent questions within the medical community. Among the most common have been their efficacy in assisting smoking cessation (Beaglehole et al., 2019; Stone and Marshall, 2019), risk that they may serve as a ‘gateway’ to youth cigarette use (Soneji et al., 2017), and the unknown impact of long-term use on health (Bold and Krishnan-Sarin, 2019). The question of health impact is of great concern due to the young age of most users and possibility of continued use throughout their lifetime. Use of any tobacco product among US youth increased in 2017 from the previous year, representing the first interruption of declining youth tobacco use rates since 1997 (Kann et al., 2018). This inflection point is entirely attributable to use of e-cigarettes, as the use of other forms of tobacco has continued to trend downward in recent years (Gentzke et al., 2019). Despite their appearance on US markets more than 10 years ago, our current knowledge regarding the long-term health impact of e-cigarettes remains largely speculative.

It is advantageous to consider the known impact of combustible tobacco cigarettes (i.e. smoking, cigarettes), given that patterns of use are similar (Keith et al., 2019; Wagener et al., 2017) and several inhaled constituents are similar between products (Schick et al., 2017). Neurovascular pathology is a well-established outcome of smoking, nearly doubling the odds of ischemic stroke worldwide (O’Donnell et al., 2016) and accounting for 7–8% of all strokes in the US (Lariscy, 2019). Smoking is also a risk factor for development of cerebral small vessel disease (van Dijk et al., 2008) and Alzheimer’s disease (Cataldo et al., 2010), and the underlying causes of several dementias including Alzheimer’s disease may involve early vascular dysfunction and blood-brain barrier (BBB) breakdown (Nation et al., 2019;

Sweeney et al., 2018; Toth et al., 2017). Beyond the vasculature, smoking may also impair neuroimmune function by acting on microglia (Brody et al., 2018, 2017).

The most prominent constituent connecting cigarettes and e-cigarettes is nicotine, which is also implicated in vascular dysfunction. E-cigarettes typically contain between 6 mg/mL and 24 mg/mL nicotine concentrations, and deliver comparable or greater amounts of nicotine to cigarettes over a given timeframe (Barrington-Trimis and Leventhal, 2018; Wagener et al., 2017). Comparable nicotine intake is observed across cigarette and e-cigarette users (Etter, 2016; Marsot and Simon, 2016), including users of high nicotine products such as Juul (Goniewicz et al., 2019; Nardone et al., 2019). Dual users titrate use to achieve an equilibrium nicotine intake across products, though there is large variability in the level attained (Dawkins et al., 2016; McRobbie et al., 2015). This observation suggests that nicotine and its metabolites serve as suitable proxies for exposure across tobacco products and in validation of pre-clinical models.

Nicotine has deleterious effects on both macro- and microvasculature. Acutely, inhalation of vaporized nicotine by human volunteers elevates blood pressure and heart rate, increases arterial stiffness, and impairs prostaglandin-associated microvascular dilation (Chaumont et al., 2018; Franzen et al., 2018). Rodent models recapitulate the increase in aortic stiffness following chronic exposure (Olfert et al., 2018), and exhibit metalloprotease upregulation and elastin degradation (Hashimoto et al., 2018; Wagenhäuser et al., 2018) which may predispose to aneurysm development. In microvasculature, nicotine reduces endothelial cell metabolism and proliferation, increases permeability, induces oxidative stress, and increases integrin expression (Schweitzer et al., 2015; Ueno et al., 2006). Increases in permeability are a consequence of decreased tight junctional (TJ) localization of Tjp1 (also known as ZO-1) (Hawkins et al., 2005, 2004) and are likely mediated by α7-homomeric nicotinic acetylcholine receptors (α7 nAChR) (Abbruscato et al., 2002). Though protracted nicotine exposure by itself is detrimental to vascular function, the combination with additional factors can have counterintuitive effects. Exposure to nicotine or α7 nAChR-agonism dampens inflammatory responses in multiple cell types including the endothelium (An et al., 2014; Krafft et al., 2013; Sharentuya et al., 2010), astrocytes (Revathikumar et al., 2016), and microglia (Li et al., 2016). These divergent findings demonstrate a highly contextual role for nicotine, dependent upon dose and possibly modified by the circadian concentration changes known to occur in human tobacco users (Hukkanen et al., 2005).

Despite not garnering the same attention as nicotine content, carbonyl compounds generated from e-cigarette refill liquid (e-liquid) vaporization is of equal concern. Acrolein, formaldehyde, and acetaldehyde are produced from propylene glycol (PG) and vegetable glycerin (VG) at vaporization temperatures (Farsalinos and Gillman, 2017; Schick et al., 2017), and are estimated to account for 80% of the health risk associated with cigarette smoking (Baumung et al., 2016; Haussmann, 2012). Carbonyl emissions are highly dependent upon conditions of use (Beauval et al., 2019; Farsalinos et al., 2015; Jensen et al., 2015), but increasing heating coil power generally increases emissions, likely from increased temperatures. Degradation products are also greater with single-coil versus double-coil designs (Sleiman et al., 2016; Talih et al., 2017). Additionally, there appears to be a modulating effect of flavor additives and nicotine, although the mechanism is not apparent.

Sucralose, a popular flavoring additive, increases aldehyde and hemiacetal emissions and several harmful compounds are formed by the combination of common flavorings with PG or VG (Duell et al., 2019; Erythropel et al., 2019). Paradoxically, the presence of nicotine appears to inhibit the formation of these compounds (Reilly et al., 2019). It is now clear that carbonyl emissions are reduced in e-cigarettes versus cigarettes (Goniewicz et al., 2017; Hecht et al., 2015; McRobbie et al., 2015); however the health consequences may remain because the biological dose response to these compounds is often non-linear (Jeelani et al., 2017). For example, acrolein produces reactive oxygen species leading to endothelial cell dysfunction at exceptionally low concentrations (Yoshida et al., 2009a) and elevates interleukin 6 and C-reactive protein production in clinical populations and experimental models (Saiki et al., 2013; Yoshida et al., 2009b).

Very little is known about the potential of e-cigarettes to cause BBB insult. In the lung, paracellular permeability is increased through p38 mitogen-activated protein kinases, Mylk3 (also known as MLC kinase) phosphorylation, and Rac1 (Schweitzer et al., 2015). However, high concentrations in the lung prevent extrapolation to systemic vasculature. Angiogenesis may increase globally within animal models (H. Shi et al., 2019), but a comprehensive exploration of end-organ injury is lacking. Immunologically, e-cigarettes cause inflammation *in vitro* (Barber et al., 2017; Rubenstein et al., 2015) and impaired lung bacterial clearance in mice (Glynos et al., 2018; Sussan et al., 2015). E-cigarettes may also alter neurotransmission within the frontal cortex and striatum and increase the glial expression of α7 nAChR (Alasmari et al., 2019, 2017). One study suggests microglial activation as a result of developmental exposure, but this may not reflect chronic use in adults (Zelikoff et al., 2018).

The present study aimed to first establish and validate a clinically relevant model of e-cigarette exposure in mice. The impact of long-term e-cigarette exposure on BBB function was assessed, including expression of vascular and inflammatory markers, permeability, and leukocyte-endothelial cell interaction. Finally, the effect of e-cigarettes on microglial activation and on several measures of affective state and cognitive function was demonstrated.

## 2. Materials and Methods

### 2.1. Animals

All experiments were conducted in accordance with the NIH Guide for the Care and Use of Laboratory Animals, ARRIVE guidelines, and followed approval by the Temple University IACUC. Male C57BL/6 mice were purchased from Jackson Laboratories (Bar Harbor, ME) and acclimated for one week prior to study entry. Mice were housed in microisolator cages on a standard 12-hour light cycle with lights on at 0700 and food/water available *ad libitum*. E-cigarette or cigarette exposure was initiated 2–3 hours following the start of the light cycle. All behavioral tests were conducted two to four hours following e-cigarette or cigarette exposure, and mice were acclimated for 30 minutes prior to testing. The timepoint for behavioral testing was chosen based on the known pharmacokinetics of nicotine in C57BL/6 mice (Siu and Tyndale, 2007). Acutely, nicotine is known to increase locomotor activity and may confound measures of anxiety and cognition which rely upon equal

locomotor activity across groups (Marks et al., 1983). Similarly, deficits in cognitive performance are observed in states of nicotine withdrawal (Saravia et al., 2019). The timepoint chosen does not represent an acutely dosed or withdrawn state and therefore allows for measure of whole e-cigarette or tobacco effect without confounding. Number of animals for each experiment was determined through power analysis and included between 3 and 10 mice per group for molecular studies and between 8 and 20 mice per group for behavioral assays. Each experiment included mice from at least two chronologically distinct cohorts of e-cigarette or cigarette exposure, and datapoints from all cohorts were included in figures.

### 2.2. E-cigarette and cigarette exposure

E-cigarette exposure was performed in a TE-2e smoking apparatus (Teague Enterprises, Woodland, CA) with 2 commercially available e-cigarettes (EVOD Mega, Kangertech, Shenzhen, China). Each e-cigarette was fitted with a 1.8Ω nichrome cotton-wick dual-coil unit (Kangertech) and tobacco-flavored e-liquid (‘Red’ Flavor, VapourV2, Peterborough, UK). E-liquid nicotine concentrations of 0 or 18 mg/mL (1.8%) were used. A four second puff (~35 mL) occurred every 30 seconds with 6 L/min total airflow. Exposure consisted of 2 hours daily, 5 days a week for 8 weeks and starting at eight weeks age. Room air controls experienced identical handling.

1R6F reference cigarettes were provided by Kentucky Tobacco Research & Development Center (Lexington, KY) and a TE-10 smoking apparatus (Teague Enterprises) provided exposure to mainstream and sidestream smoke. Settings conformed with ISO smoking regimen (Chae et al., 2017), with two second puffs of thirty five milliliter total volume. Two cigarettes burned concurrently with twenty-eight seconds interpuff duration and approximately 3.7 L/min airflow. Flow was adjusted to maintain target total particulate matter (tpm) of 100 $mg/m^3$. In pilot experiments, a range of tpm concentrations were correlated with serum cotinine concentration. This concentration of tpm produced serum cotinine equivalent to our e-cigarette model, and was used in all subsequent work to ensure comparable levels of exposure in cigarette-exposed groups (Figure 1B). Exposure age and regimen were matched to e-cigarette studies.

Mice were transferred to polycarbonate cages of identical dimension to their housing cages for the duration of exposure, but with wire-top lids to allow for free passage of smoke and vapor. Food and water were not available during the exposure period due to risk of contamination and subsequent exposure to e-cigarette or smoke condensates by oral route.

### 2.3. Blood collection and cotinine LC-MS

Submandibular bleed occurred 1-hour post-exposure, at weeks 1, 3, 5, and 7 of exposure. Microextraction of nicotine and cotinine was performed as previously described (Yasuda et al., 2013). Briefly, 10 μL serum from each mouse was diluted 1:5 and 5M sodium hydroxide was added. Internal standard provided a final concentration of 0.5μM deuterated analytes. Chloroform was used for extraction and recovery utilized 0.1M hydrochloric acid. The Wistar Metabolomics Facility (Philadelphia, PA) performed quantification by Vanquish Horizon UHPLC system (Fisher Scientific, Waltham, MA) coupled to Q-Exactive HF-X

mass spectrometer (Fisher Scientific). Elution of nicotine and cotinine were observed at 1.2 minutes and 1.5 minutes, respectively.

### 2.4. E-liquid nicotine LC-MS/MS

Prior to use, all e-liquid formulations were diluted 1:200 and submitted for analysis of nicotine concentration by a clinically-accredited laboratory (NMS Labs, Horsham, PA; Test Code 3150FL). This approach provided a lower limit of detection of 0.5 μg/mL for the original e-liquid formations.

### 2.5. Cerebral microvessel isolation and RNA-seq

Mice were euthanized by decapitation under isoflurane anesthesia 24 hours following the last e-cigarette or smoke exposure. Whole brain was placed in 4°C MCDB 131 medium (Fisher Scientific) with 15 μL/mL RNase Inhibitor (Fisher Scientific). Microvessel isolation was carried out as described by our lab (Bernstein et al., 2019) with modifications suggested by Lee and colleagues (2019). All steps were carried out in a cold room and all solutions were supplemented with 3 μL/mL RNase Inhibitor. Tissue was dounce homogenized, pelleted, and resuspended in 17.5% dextran (Sigma Aldrich, St. Louis, MO). Centrifugation at 4400x*g*, 15 min, 4°C caused separate pelleting of myelin and vessels along opposite surfaces. The vessel pellet was resuspended in 1% bovine serum albumin (BSA) in Hank's balanced salt solution, agitated via serological pipette, and passed through a 40-μm filter. Vessels were recovered from the filter with 4% BSA, pelleted, and snap frozen. RNA isolation was performed using TRIzol reagent (Fisher Scientific) and characterized via NanoDrop 2000 spectrophotometer (Fisher Scientific). Samples with a 260/280 wavelength ratio outside of the range 1.8 to 2.0 were excluded. Unpooled isolates from 3–4 mice per group were used in subsequent sequencing steps.

Isolated RNA was provided to the Fox Chase Genomics Core, where it was reverse transcribed, and sequenced via HiSeq2500 (Illumina, San Diego, CA) with Nextera-based primers and reagents. Each sample was sequenced twice to provide two technical replicates per biological replicate. The 50-nucleotide end reads were aligned to the mouse genome (GRCm38.p6) using bowtie2. Mapped reads were normalized and DEG were identified using the R package DESeq2 (Release 3.10). Sequencing data were deposited in NCBI's GEO database (GSE142400).

### 2.6. Histology

The left hemisphere of brain and lung post-caval lobe were fixed in Poly/LEM (Polysciences Inc, Warrington, PA), paraffin embedded, and 5 μm sections collected to include lung, brain neocortex (frontal and parietal), and basal ganglia. One section was collected for each antigen and used with the following primary antibodies: rabbit anti-Iba1 (Polyclonal, 1:500, Wako/Fujifilm Laboratory Chemicals, Valhalla, NY), mouse anti-Claudin 5 (4C3C2, 1:50, Invitrogen, Carlsbad, CA), rabbit anti-Occludin (Polyclonal, Novus Biological, Centennial, CO), mouse anti-Glut1 (SPM498, 1:500, Abcam, Cambridge, UK). Peroxidase detection used Vectastain Elite ABC HRP kit (Vector Laboratories, Burlingam, CA), followed by hematoxylin counterstain. Full sections were captured by Aperio AT2 slide scanner (Leica Biosystems, Wetzlar, Germany).

### 2.7. Image analysis

Whole hemisphere images were manually annotated for regions of interest (ROI) by a blinded observer within NIS-Elements (Nikon, Tokyo, Japan). A binary rendering of peroxidase-reactive regions was generated using the General Analysis 3 module and used for all further measurements. For vessel-localized antigens (Claudin 5, Occludin, Glut1) the percent peroxidase-positive ROI area was calculated. Densitometry of the red channel was also examined as this component was most sensitive to the presence of peroxidase. Microglial analysis utilized smoothing and skeletonization of binary renderings, followed by calculation of total process length and coverage per unit area, total microglial cell density, territory covered per microglia, and average microglial branching. In the case of lung tissue, a binary rendering of total area excluding alveolar space was quantified using an absolute intensity threshold.

### 2.8. BBB permeability assay

NaF and TMR-dextran served as tracers, while cyanine 5-conjugated LEL served as a vascular marker. All tracers and markers were injected retroorbitally just prior to euthanasia. Mice were then transcardially perfused with cold phosphate-buffered saline. Meninges were removed, and the left hemisphere was embedded in OCT. 200 μm sections included parietal cortex, caudate nucleus, thalamus, and hippocampus which were immediately imaged via A1R confocal microscope (Nikon). ROI were annotated by blinded observer, then mean tracer intensities were calculated for each ROI. Residual tracer in the vasculature was excluded by use of the LEL marker to exclude vascular space. All measurements were normalized against plasma fluorescence of tracers.

### 2.9. Intravital imaging

An account of our group’s approach to cerebral intravital imaging has been detailed previously (Zuluaga-Ramirez et al., 2015) and will be described more broadly here. Mice underwent implantation of a cranial window and icv cannula six days prior to the intravital imaging session. Anesthesia was performed with isoflurane and an aperture was created in the right parietal bone using a high-speed dental drill (CellPoint Scientific, Gaithersburg, MD). A 2.5 mm circular window was created over the lateroposterior aspect of the right parietal bone and dura matter was deflected outward without disruption of underlying arachnoid. A glass coverslip was affixed over the opening and a 33g guide cannula (PlasticsOne, Roanoke, VA) was affixed to the aperture.

Immediately following exposure, pial vessels of mice were baseline imaged using a Stereo Discovery V20 epifluorescence microscope (Carl Zeiss AG, Oberkochen, Germany) with AxioCam MR digital camera (Carl Zeiss AG). Previous data from our lab (unpublished) have found no differences in leukocyte rolling or adhesion immediately before versus after e-cigarette and smoking exposure. 0.05% Rhodamine 6G and 0.5% fluorescein isothiocyanate (FITC)-dextran 70 kDa were injected retroorbitally prior to imaging. Three to four sites from each window were selected for video imaging. 5 μg Tnf was then injected icv via previously placed cannula. Repeat imaging occurred 2 hours following injection of Tnf. Imaris software (Bitplane, Belfast, Northern Ireland) was used for leukocyte quantification. Due to occasional respiration-associated movement of imaging window relative to the scope,

adherent leukocytes were defined as spots which did not exhibit a change in location ≥ 40 μm for the duration of the video. All other leukocytes confined to the vessel space were classified as rolling.

### 2.10. Reverse transcription quantitative polymerase chain reaction

RNA was extracted from post-caval lung tissue using TRIzol reagent (Fisher Scientific) according to manufacturer instructions. NanoDrop 1000 spectrometer (Fisher Scientific) was used to quantify RNA concentration and purity. cDNA was then produced from 250 ng RNA using a High-Capacity cDNA Reverse Transcription Kit (Fisher Scientific). Quantitative polymerase chain reaction (qPCR) was performed on a QuantStudio 3 instrument using Fast Advanced Master Mix Reagents (Fisher Scientific) and a concentration of 1 ng cDNA per reaction. The Ct algorithm was used to provide relative quantitation based on a Gapdh loading control, and fold change values were expressed relative to the average expression of room air mice.

### 2.11. Plasma cytokine ELISA

Blood plasma was collected from the inferior vena cava of anesthetized mice prior to euthanasia and stored at −80°C prior to quantitation. A V-PLEX Proinflammatory Panel 1 Mouse Kit (Cat K15058D, Mesoscale Discovery, Rockville, MD) was used according to manufacturer's instructions.

### 2.12. Novel object recognition test

Novel object recognition test (NORT) was conducted during exposure week 7 as established by Shi et al (2019). The paradigm consisted of a habituation phase on day 1 and familiarization and test phases on day 2. During habituation, mice were allowed 30 minutes in the empty chamber. For familiarization, two identical objects were placed in adjacent corners and 10 minutes were provided for exploration. Mice were then single-housed for 30 minutes. One object was replaced with a novel object and mice were returned to the chamber for a 10-minute test. Videos were scored by blinded observer. Object investigation included time with nose pointed toward the object and distance ≤ 1 cm. Discrimination index (DI) was defined as follows: (*time exploring novel object – time exploring familiar object*)/*total time exploring objects* x 100%.

### 2.13. Y-maze spontaneous alternation task

The Y-maze spontaneous alternation task (SAT) is often used to evaluate spatial working memory, a hippocampus-dependent domain, and relies upon the innate curiosity of mice to explore arms which they least recently visited (Kraeuter et al., 2019). SAT was performed as previously described by our group (Rom et al., 2019) during exposure week 7. The maze consists of 3 arms separated by 120° and a central entry zone. Mice were allowed 10 minutes exploration time and order of entries was scored by a blinded observer. Percent spontaneous alternation examines complete successive triplets in the arm entry order (i.e., if arm entry sequence is $X_1$ -> $X_n$, triplets include $X_1X_2X_3$, $X_2X_3X_4$…$X_{n-2}X_{n-1}X_n$). Percent spontaneous alternation was defined as the percent of these triplets which included all three

arms of the maze. Total arm entries were scored as an index of total ambulatory activity; and mice with less than 6 total arm entries were excluded.

### 2.14. Elevated plus maze

To provide a measure of anxiety-associated behavior, mice were evaluated by elevated plus maze (EPM) paradigm (Holliday et al., 2016) during week 6 of exposure. Mice were placed in the central zone and allowed 10 minutes of exploration time. Videos were scored by a blinded observer, and total time spent in open arms was calculated.

### 2.15. Open field assessment

Total ambulatory activity was evaluated during a ten-minute trial in open field apparatus during exposure week 6. Total ambulatory distance was quantified by AnyMaze software (Stoelting Co, Wood Dale, IL) as a measure of locomotor activity.

### 2.16. Statistical analysis

All experimental measurements are expressed as mean ± SE. Shapiro-Wilk test was applied to test the assumption of data distribution normality, then parametric tests were applied. One-way ANOVA with two-tailed Holm-Sidak post-hoc was used, except for intravital imaging, permeability, and histology, where two-way ANOVA was applied to examine the interaction of exposure with Tnf or with brain region. p-value of ≤0.05 was considered significant.

### 2.17. Data availability

The data that support the findings of this study are available from the corresponding author, upon reasonable request.

## 3. Results

### 3.1. Smoke and e-cigarette inhalation models produce clinically relevant nicotine intake and delay growth

To determine the clinical relevance of our model and facilitate comparison between e-cigarette and smoking groups, we assessed changes in body weight and serum cotinine. Delayed weight gain in mice exposed to cigarettes is well established, and nicotine in e-cigarettes may have a similar effect (Lerner et al., 2015; H. Shi et al., 2019; Tsuji et al., 2011). Timepoint and exposure had a significant effect on body weight, but these factors did not interact (Fig. 1A). All groups had comparable starting weight, but cigarette-exposed mice (Cig) weighed less than other groups at subsequent timepoints. This effect was statistically significant only at week 4 (room air, m=28.25, standard error of the mean (SE) 0.41; cigarette, m=26.83, SE 0.38 g; p=0.0227). Nicotine-containing e-cigarette exposure (EC1.8%) did not significantly impact body weight at any recorded timepoints.

Cotinine is a clinical biomarker of nicotine exposure and the 1-hour post-exposure timepoint has been used in previous pre-clinical work (Hage et al., 2017; Sussan et al., 2015). In humans, serum cotinine is generally within 100 to 200 ng/mL and is comparable across cigarettes and e-cigarettes. We evaluated cotinine throughout exposure (Fig. 1B), finding

both Cig (m=142.8 ng/mL, SE 28.64) and EC1.8% (m=134.0 ng/mL, SE 21.6) groups were within a clinically relevant range. EC1.8% and Cig group did not differ statistically, supporting similar nicotine delivery. E-liquids from EC0% and EC1.8% were also tested for nicotine content. EC1.8% e-liquids contained the listed concentration (18.0 mg/mL), while EC0% e-liquids had no detectable nicotine. In aggregate, these findings suggest parallels between the experimental parameters selected for this study and the attributes observed in human smokers and e-cigarette users.

### 3.2. Tight junction- and transporter-associated mRNA expression is influenced by nicotine-free e-cigarettes

Following model validation, cerebral microvessel mRNA was sequenced to identify differentially expressed genes (DEG). Surprisingly, EC0% exposure resulted in substantially more DEG than in EC1.8% or Cig. A total of 2,163 genes were upregulated and 2,281 downregulated by EC0% exposure, representing a respective 5.5% and 5.8% of the 39,179 genes surveyed (Fig. 2A). In contrast, 311 (0.8%) and 863 (2.2%) genes were up- and downregulated following EC1.8% exposure and only 529 (1.4%) and 384 (1.0%) were up- and downregulated after exposure to Cig (Fig. 2B & 2C). A substantial proportion of DEG associated with EC1.8% were shared with EC0% exposure. Specifically, 90 of 311 genes upregulated (28.9%) and 383 of 863 genes downregulated (44.4%) by EC1.8% exposure were common to EC0% (Fig. 2D & 2E). In contrast, only 25/539 (4.7%) upregulated and 4/384 (1.0%) downregulated by Cig exposure were common to EC0%. This is consistent, given that EC1.8% versus EC0% e-liquids vary only in nicotine content, while cigarettes contain a distinct mixture of products. However, global changes following EC0% were attenuated with nicotine (EC1.8%) suggesting an antagonistic or moderating contribution of nicotine in this context.

To examine DEG with known BBB relevance, previously published gene sets (Munji et al., 2019) were cross-referenced with DEG in all exposure groups. Most notable were genes associated with TJ complexes, those facilitating drug efflux or the active transport of key nutrients, and BBB-enriched immune response genes (Fig. 3A). Metadherin (Mtdh) is recruited to TJ during complex maturation and overexpression may downregulate excitatory amino acid transporters (e.g. Slc1a2) and activate NF-κB complex. *Mtdh* is increased 1.41-fold (p=9.45e-5) in EC0%-exposed microvessels, though no differences were apparent in EC1.8%- or Cig-exposed groups. Occludin (*Ocln*) expression was significantly reduced in EC0% animals (0.50-fold, p=9.09e-11) (Fig. 3B). *Ocln* expression trended upward in EC1.8% and Cig groups, but these findings were nonsignificant (EC1.8%, 1.11-fold, p=0.7494; Cig, 1.52-fold, p=0.0590). Among transporters, several genes with critical roles related to CNS metabolism were impacted. Monocarboxylate transporter 1 (Slc16a1) transports lactate, pyruvate, and branched-chain amino acids and is upregulated by e-cigarettes regardless of nicotine content (EC0%, 1.30-fold, p=0.0001; EC1.8%, 1.80-fold, p=0.0010; Cig, 1.03-fold, p=0.9034) (Fig. 3B). BBB glucose transport requires exclusively Glut1 (encoded by *Slc2a1*), which is diminished following EC0% (0.45-fold, p=1.61e-11) but increased following Cig (1.59-fold, p=0.0010) (Fig. 3B). Interestingly, changes in *Slc2a1* were not seen in the EC1.8% group (1.044-fold, p=0.9407). Lastly, several BBB-enriched immune-associated genes exhibited significant transcriptional changes. Cigarette exposure

triggered upregulation of inflammation-associated transcripts such as *Cxcl12* (1.42-fold, p=0.0181) and *Ifnar1* (1.28-fold, p=0.0381). Integrin alpha 4 (*Itga4*) was uniquely increased in the EC1.8% group (1.39-fold, p=0.0126) (Fig. 3B) but largely unchanged in other groups (EC0%, 1.00-fold, p=0.8276; Cig, 1.12-fold, p=0.5706). Loss of TJ- and transport-associated transcripts specifically following EC0% provides evidence for a detrimental effect of non-nicotinic e-cigarette constituents. We can further conclude that the transcriptional impact of e-cigarettes on microvessels is unique from that of traditional tobacco products.

### 3.3. Expression of TJ proteins are disrupted by e-cigarette or cigarette exposure

Next, we asked whether exposure had an impact beyond the transcriptomic level. Specifically, appropriate trafficking of TJ proteins is essential for low paracellular permeability. Coronal sections containing areas of the frontal cortex and basal ganglia were peroxidase-labelled for either Occludin or Claudin 5. Expression of Occludin at vessel TJs was significantly decreased in the cortex (Fig. 4E–H, 4I). This was independent of nicotine, as both EC0% (m=0.677, SE 0.095, p=0.0107) and EC1.8% (m=0.697, SE 0.034, p=0.0128) induced similar decreases versus room air (m=1, SE 0.087). Cig elicited a similar decrease (m=0.679, SE 0.065, p=0.0107). Similar trends in basal ganglia did not reach statistical significance (Fig. 4A–D, 4I) (EC0%, m=0.774, SE 0.073, p=0.1398; EC1.8%, m=0.836, SE=0.058, p=0.4098; Cig, m=0.900, SE 0.068, p=0.6986).

Unlike the TJ-exclusive localization of Occludin, Claudin 5 was seen throughout the vessel (Fig. 5A–H). Claudin 5 distribution was not appreciably different across exposure groups or regions (Fig. 5I). Although Claudin 5 expression is not impacted, loss of a single TJ component is often enough to impact permeability.

### 3.4. BBB permeability is increased following nicotine-free e-cigarette exposure

Given the ubiquitous effect on TJ localization, two exogenous tracers were used to directly observe changes in permeability. Tracers of two distinct sizes were chosen (sodium fluorescein (NaF), 376 Da; tetramethylrhodamine (TMR) -dextran, 10 kDa). Variability was driven by exposure for both NaF (Fig. 6M) and dextran (Fig. 6N). In the EC0% group, deposition was increased across all regions (Fig. 6D–F, O). These differences were significant within thalamic nuclei (NaF, m=1.799, SE 0.356, p=0.0092; dextran, m=2.066, SE 0.488, p=0.0257). For each exposure group, observed permeability changes were consistent across all brain regions, but the magnitude was greatest in medial structures such as the thalamus and hippocampus. Previously reported regional responses to insult are largely consistent with this finding (Villaseñor et al., 2017). Tracer deposition following EC1.8% exposure trended downward (Fig. 6G–I), which may suggest a reversal of e-cigarette effect by nicotine, even generating a less permissive barrier than in naïve animals. Cig treatment did not have a conclusive effect (Fig. 6J–L). These data demonstrate that functional increases in permeability are unique to EC0% exposure and additional factors beyond Occludin can modify BBB response.

### 3.5. Exposure to e-cigarettes or cigarettes decreases expression of Glut1 within the parietal cortex

Prior reports indicate Glut1 decreases in response to *in vitro* cigarette treatments (Prasad et al., 2017). Based on the observed reduction of Glut1 mRNA following EC0% exposure, changes in expression were investigated. Glut1 maintained relatively consistent densitometry, but Glut1 vessel coverage was modulated in response to exposure. We therefore quantified percent immunopositive area (Fig. 7I). Decreased expression was specific to cortical structures and was generalizable to all exposure groups including EC0% (m=0.307, SE 0.093, p=0.0018), EC1.8% (m=0.481, SE 0.069, p=0.0137), and Cig (m=0.319, SE 0.042, p=0.0007) (Fig. 7A–D). The finding here that Glut1 expression decreases *in vivo* following Cig exposure is complementary to previous findings in cell culture, and this finding appears generalizable to e-cigarettes regardless of nicotine content.

### 3.6. Tumor necrosis factor (Tnf)-induced leukocyte adhesion is aggravated by prior exposure to cigarettes or e-cigarettes

The BBB provides an interface between the peripheral immune system and immune-privileged CNS tissues. Further, the magnitude of blood-leukocyte interaction and the induction of permeability are frequently correlated (Rom et al., 2015a). We employed intravital imaging with intracerebroventricular (icv) injection of Tnf to induce an aseptic meningitis (Zuluaga-Ramirez et al., 2015) and determine whether chronic inflammation may ‘prime’ for an increased acute response (Fig. 8I). Virtually no leukocytes were observed prior to administration of Tnf regardless of group. Following Tnf injection, leukocyte margination was elevated in all exposure groups versus room air (m=11.699, SE 0.486) (Fig. 8A & 8B, Supplemental Video 1). This included increases for EC0% (m=29.416, SE 2.506, p<0.0001), EC1.8% (m=19.185, SE 1.582, p=0.0037), and Cig (m=25.001, SE 2.347, p<0.0001) (Fig. 8C–H, Supplemental Video 1). Furthermore, the EC0% group was significantly increased beyond EC 1.8% (p=0.0001) and Cig (p=0.0352) groups, similar to our permeability observations where only EC0% mice were affected. Cig group margination was also elevated beyond EC1.8% mice (p=0.0175). Upon further subdivision, exposure did not have a substantial effect on leukocyte rolling (Fig. 8J). Differences between EC1.8% (m=3.391, SE 0.525) and Cig (m=1.966, SE 0.448, p=0.0321) were identified but were of unclear practical significance. Adherent leukocytes largely mirrored findings of total margination (Fig. 8K). Adherence was increased for EC0% (m=26.843, SE 1.871, p<0.0001), EC1.8% (m=15.794, SE 1.492, p=0.0010), and Cig (m=23.035, SE 2.057, p<0.0001) relative to room air (m=8.979, SE 0.391). Differences between EC0% versus EC1.8% (p<0.0001) or Cig (p=0.0307), and EC1.8% versus Cig (p=0.0005) also remained.

### 3.7. Pulmonary macrophages are increased by exposure to nicotine-containing e-cigarettes or cigarettes

Given the increased adhesion of peripheral leukocytes to brain endothelium, we further examined whether increased inflammation in other organ systems could contribute to our observations. E-cigarettes and cigarettes first interface with lung tissue and we therefore began by quantifying alveolar macrophage abundance (Supplemental Fig. 1A–E). Initial examination revealed clusters of macrophages localized around bronchioles and vasculature,

and regions within 100 μm of these structures were selected for further analysis. Surrounding bronchioles, the number of macrophages was increased in EC1.8% exposed mice (m=2.200, SE 0.2748) when compared with all other groups, including room air (m=0.2320, SE 0.0970, p<0.0001), EC0% (m=0.1057, SE 0.0380, p<0.0001), and Cig (m=0.6386, SE 0.2103, p<0.0001). Similarly, a significantly greater abundance of peri-vascular macrophages was observed in EC1.8% exposed mice (m=2.630, SE 0.2329) compared with room air (m=0.2340, SE 0.0755, p<0.0001), EC0% (m=0.1329, SE 0.2329, p<0.0001), and Cig (m=0.8886, SE 0.2098, p<0.0001). Additionally, peri-vascular macrophages were elevated in Cig exposed mice compared with room air (p=0.0226) and EC0% (p=0.0064). The observed increase in macrophage accumulation warranted further investigation into the expression of cytokines which may be associated with their recruitment or phenotype, and therefore expression of common cytokines within pulmonary tissue was explored. EC0% exposed mice showed a small but significant increase in the expression of Il1b mRNA over other groups (EC0%, m = 1.838, SE 2.112; room air, m=1.000, SE 1.707, p=0.0463; EC1.8%, m=0.4449, SE 2.371, p=0.0013; Cig, m=0.5194, SE 1.243, p=0.0009), although this finding did not correlate with measures of macrophage abundance. Measures of other cytokine mRNAs (Il1b, Il4, Il6, Il13) were unchanged across groups. In order to further characterize the systemic impact of exposure, blood plasma was collected and assessed for the concentration of multiple pro-inflammatory and anti-inflammatory factors. All cytokines measured were either unchanged (IL-5, IL6, KC/GRO, TNF), or below the lower limits of detection (IFN-γ, IL-1b, IL-2, IL-4, IL-10, IL-12).

### 3.8. Microglial arborization is increased within the striatum by nicotine-containing e-cigarettes

Next, we investigated whether neuroinflammatory changes existed beyond the BBB and within the parenchyma itself. Sections were stained for Iba1 (ionized calcium binding adaptor molecule 1, encoded by *Aif1*), a constitutive marker of microglia. Several morphometric parameters were analyzed including total Iba1-positive area, total process length, total microglial cell density, and average branch intersections per microglia. Iba1-positive area was elevated only within the basal ganglia of the EC1.8% group (m=2.703, SE 0.570) in EC0% (m=1.303, SE 0.420, p=0.0440) and Cig (m=1.452, SE 0.151, p=0.0440) (Fig. 9E–H). Increased Iba1-positive area may be a result of increased arborization or an elevation of the total number of microglia present. To differentiate, process length with exclusion of cell body regions was quantified, and largely mirrored Iba1-positive area (Fig. 9J). In the basal ganglia, arborization was enhanced in EC1.8% exposed mice (m=2.155, SE 0.378) relative to EC0% (m=0.801, SE 0.213, p=0.0065) and Cig (m=1.101, SE 0.120, p=0.0144). In contrast, EC1.8% exposed mice did not have increased microglial cell density (Fig. 9K), although in the cortex EC0% there was an increase (m=3.744, SE 0.432) as compared to Cig (m=1.850, SE 0.261, p=0.0347). Lastly, the nature of arborization was characterized by quantification of total branch points within visible whole microglia (Fig. 9L). No discrete differences were observed, suggesting that increased arborization is likely a result of greater area surveilled and not a ‘bushier’ morphology associated with partial activation.

### 3.9. Deficits in NORT are induced by nicotine-free e-cigarette exposure

To understand the functional consequences of these findings, several behavioral assessments were carried out. Y-maze was conducted as a preliminary measure of spontaneous exploratory behavior. The correct alternation percentage was not impacted by exposure to any of the tobacco products tested (Fig. 10A). Total number of arm entries was noted to control for locomotion and did not differ by group (Supplemental Fig. 2A). NORT provided a further look at short-term memory (Fig. 10B). Performance of EC0% exposed mice (m=-7.979, SE 15.14) was impaired in relation to room air (m=46.22, SE 8.432, p=0.0061), EC1.8% (m=58.47, SE 9.627, p=0.0013) and Cig (m=41.41, SE 10.61, p=0.0172). Exploration time and initial object preference were not confounders of this measure (Supplemental Fig. 2B & 2C). We further investigated the impact on anxiety-related behavior via EPM (Fig. 10C). Cig exposure had an anxiogenic effect (m=4.322, SE 0.9570) relative to room air (m=13.50, SE 1.546, p=0.0003) and EC1.8% (m=10.78, SE 1.227, p=0.0214). Finally, open field provided additional assurance that acute nicotinic motor stimulation (Marks et al., 1983) was not a confounder. Total distance travelled did not significantly differ between groups (Fig. 10D). Taken together, these data demonstrate a damaging effect of nicotine-free e-cigarettes on cognition, which is not confounded by the known pharmacological profile of nicotine products.

## 4. Discussion

Our findings represent the first characterization of e-cigarette-associated neurovascular alternations in an animal model, and bridge a current knowledge gap between clinical investigation of e-cigarette users and mechanistic studies in cell culture-based systems. Given the short history of use by human populations, this type of model is uniquely positioned to characterize e-cigarette-associated pathology which may not be identifiable by clinical observation for several decades. However, recapitulation of the diverse use conditions within a standardized model requires consideration of evolving demographics. Essentially all e-liquids in use today contain flavoring additives, and tobacco flavors remain popular among a substantial number of users (Landry et al., 2019; Romberg et al., 2019). Based on this, we utilized tobacco-flavored formulations and chose a nicotine concentration (1.8%) with relevance to the largest proportion of users. In conjunction with serum cotinine levels which match clinical findings and ensure equivalent exposure between distinct tobacco products (e-cigarette versus cigarette), a meaningful basis for comparison has been established. In order to maintain equivalence across exposure groups, the cigarette smoke density used in the present study was substantially lower than much of the previous literature which sought to induce COPD-associated pathology within a short timeframe (Tsuji et al., 2011). This approach provided parity in nicotine delivery, and may explain the lack of robust weight loss in the cigarette-exposed group by post-hoc testing, although a significant main effect of exposure was observed.

Following model validation, both nicotine-dependent and -independent neurovascular consequences of e-cigarette exposure were apparent. The transcriptomic profile of e-cigarette exposure was distinct from that of cigarettes and exhibited nicotine-dependent differences. Although e-cigarettes and cigarettes contain many common constituents, the

transcriptomic overlap between these groups was minimal. This would suggest that factors unique to cigarettes may overshadow the effect of common constituents. Despite the highly divergent transcriptomic data, exposure to any of the tested tobacco products had similar effects at the protein level, both in relation to TJ protein localization and glucose transporter coverage across the vasculature. However, the functional consequences of tight junction dysregulation were not uniform throughout groups, as observed by extravasation of BBB permeability markers. Based on this, we can assume that additional factors may modify the effect of Occludin dysregulation on paracellular permeability.

Regional heterogeneity in several factors was also identified, both at baseline and in response to tobacco product exposure. Given the diffuse nature of tobacco product exposure, it is likely that this heterogeneity reflects differences in susceptibility and response to insult across regions. Loss of Occludin localization was most pronounced within cortical regions, and did not correlate regionally with permeability based on the extravasation of tracers. This may be explained by an excess of baseline Occludin expression in cortical regions, meaning a loss of expression or proper localization may not be associated with the same functional consequences as in other regions. Additionally, while Occludin expression is frequently examined as a correlative measure of BBB dysfunction, the genetic loss of Occludin does not directly lead to increased permeability and loss of TJ integrity (Saitou et al., 2000). It is likely that other unexamined factors also contribute to the differences in permeability observed here. One such possibility is that the observed Occludin downregulation is an indicator of broader cytoskeletal rearrangement and loss of circumferential actin, as there is a strong correlation of Occludin expression with cytoskeletal organization in endothelial cells (Kuwabara et al., 2001). Our group and others have demonstrated the involvement and importance of Rho-mediated cytoskeletal rearrangements in endothelial-leukocyte interaction, and blockade of GTPase activity can prevent associated loss of Occludin and Claudin 5 localization (Persidsky et al., 2006; Rom et al., 2015b). More broadly, numerous phosphorylation and post-translational modification events can produce forms of Occludin which are deleterious to the TJ assembly (Cummins, 2012), and it is well understood that adherens junction integrity is a necessary prerequisite for TJ function (Abbott et al., 2010). Further mechanistic studies are required to better understand the molecular nature of the functional deficits observed here.

The cortical loss of Glut1 coverage is of particular interest in conjunction with measurement of leukocyte extravasation, which was observed in the pial and superficial parenchymal vessels of the parietal cortex. These findings, either alone or in combination, may be expected to contribute to cortical dysfunction and functional deficits.

Contrary to initial expectation, e-cigarette emissions without nicotine had a robust effect that often exceeded its nicotinic counterpart. This was particularly evident with respect to reduced gene expression of critical BBB-associated genes, increased paracellular permeability, and impaired cognition. In these cases, the corresponding nicotine group was unchanged from room air. Though all forms of e-cigarette and cigarette exposure impacted leukocyte margination, nicotine-free e-cigarette exposure exhibited the most robust effects by far. Although counterintuitive, these findings coincide with previous work in cell culture which demonstrates an exaggerated complement deposition and CD35 expression on

endothelial cells following treatment with nicotine-free formulations when compared to nicotine-containing counterparts (Barber et al., 2017; Rubenstein et al., 2015). Nicotine-free e-cigarettes have also demonstrated impact on vascular function in human never-smokers, although this effect is apparently not observable with exposure to vehicle alone in regular tobacco users (Caporale et al., 2019; Chaumont et al., 2018). Further study is needed to determine whether the moderating influence of nicotine in this context is due to reduced generation of harmful byproducts (Reilly et al., 2019) or a functional antagonism of vaping-associated pathophysiology. Regardless, the deleterious impact of nicotine-free e-cigarette use has significant implications for the use of e-cigarettes as alternative delivery devices for cannabinoids or illicit substances.

Observed changes in paracellular permeability were seemingly reversed by the addition of nicotine, and even trended toward a decrease versus room air values in the nicotine-containing e-cigarette group. These findings demonstrate that nicotine exposure can have a highly divergent effects depending on the context and pattern of exposure. Although the available *in vivo* literature on BBB permeability would predict a disruptive effect of nicotine (Hawkins et al., 2004), this finding was determined following chronic subcutaneous dosing and other work has demonstrated a rebound inflammatory effect following this mode of exposure (Saravia et al., 2019). In contrast, acute nicotinic agonism has a reported anti-inflammatory effect in models of disease (Krafft et al., 2013; Sharentuya et al., 2010). The present model results in circadian fluctuation of nicotine dose which is not analogous to either of the previously described dosing strategies. In this context, it appears that nicotine plays an anti-inflammatory and BBB-protective role as evidenced by the findings of reduced leukocyte margination. This is most likely due to action at α7 nAChR, although this was not addressed in the present study and further investigation is warranted.

The systemic nature of tobacco-associated disease is well known, and likewise it is unlikely that inflammatory effects observed at the BBB are occurring in isolation. It is possible that rather than resulting from direct action of circulating e-cigarette constituents, these changes may be a reflection of the pulmonary and immune reaction to exposure, and subsequent signaling from these tissues. On this basis, we explored the macrophage abundance in pulmonary tissue and observed a bronchial and vascular cuffing pattern consistent with observations in previous literature (Braber et al., 2010). Interestingly, elevated accumulation of macrophages was associated with nicotine-containing products, while findings in nicotine-free exposed mice largely resembled that of room air. A similar effect has been observed following short-term e-cigarette exposure (Bahmed et al., 2019), where nicotine-containing e-cigarette, but not vehicle, increased macrophage accumulation. However, the increased presence of immune cells was not mirrored by increased pulmonary cytokine expression, nor were circulating cytokines impacted. The only notable finding was an increase of Il1b following nicotine-free exposure, which is unexpected given the lack macrophage accumulation in this group. This is not altogether unprecedented, as other groups using similar non-acute exposure regimens have reported a similar lack of cytokine elevation in bronchoalveolar lavage fluid (Larcombe et al., 2017), and alveolar macrophages from smokers exhibit a blunted response to pro-inflammatory stimuli (Chen et al., 2007). Further, it has been reported that despite increasing numbers of pulmonary immune infiltration, e-cigarette exposed mice may have a compromised response to pathogens

associated with a functionally impaired immune response (Sussan et al., 2015). Based on our data it is unlikely that the observed cerebrovascular findings result from changes in systemic cytokines, but the possibility of a cell-based or other signaling mechanism between the lung and the brain cannot be ruled out.

Despite parallels between the described model and human use, the accelerated metabolism of nicotine in mice is a potential caveat that must be considered (Siu and Tyndale, 2007). Circulating levels of nicotine decay rapidly in this setting and are virtually undetectable by sixteen hours post-exposure. While this is somewhat inconsistent with the low levels that persist in humans overnight (Hukkanen et al., 2005), the circadian variation in blood nicotine is roughly recapitulated by this model. Furthermore, the contribution of non-nicotinic e-cigarette components and metabolites must be considered, as are pharmacokinetically uncharacterized and may persist in circulation much longer. These compounds exert a considerable pathological effect based on the findings presented here. It should also be noted that only male mice of a single strain were evaluated in this work. Although several strains have been used in the evaluation of smoke exposure, the C57BL/6 inbred strain is most commonly used in existing cigarette and e-cigarette literature (Alasmari et al., 2017; Kuntic et al., 2019; Lee et al., 2018; Olfert et al., 2018). Comparisons have demonstrated susceptibility of C57BL/6 mice to pulmonary pathology relative to other strains (Bartalesi et al., 2005; Tsuji et al., 2011), although rodents as a whole exhibit a greater resistance to the pro-oxidant and pro-inflammatory effects of smoke exposure. The C57BL/6 strain was chosen to provide greatest concordance with existing literature, and may also maximize clinical relevance while avoiding specific gene knockout or deficit models (Yun et al., 2017). Additionally, the described findings may not be generalizable across sexes, as there is a known impact of estrogen on atherosclerosis and other smoking-related diseases (El-Mas et al., 2012; Middlekauff et al., 2013). Male mice were chosen as a starting point for understanding e-cigarette impact, as use of both cigarettes and e-cigarettes is more common in males (Agaku et al., 2014; Stallings-Smith and Ballantyne, 2019).

In summary, these findings provide evidence that long term use of e-cigarettes may negatively affect neurovascular health and contribute to cognitive dysfunction, regardless of nicotine content. The impact of e-cigarette use is often equivalent to comparable exposures of combustible tobacco, and may even be uniquely deleterious in some contexts. Future studies are needed to further understand the specific constituents and byproducts which are implicated and determine the mechanisms which mediate these effects.

## Supplementary Material

Refer to Web version on PubMed Central for supplementary material.

## Acknowledgements

The authors are grateful to several individuals for their role in making this project possible. Dr. Hsin-Yao Tang and the Wistar Institute metabolomics core provided technical assistance and insight during development of LC-MS methodology. Dr. Beata Kosmider provided equipment, initial training, and expert perspective for establishment of the e-cigarette exposure model. Image analysis approaches were developed in consultation with Roshanak Razmpour.

## Funding

This work was supported in part by NIH grants T32DA007237 (NH) and R01DA040619 (YP).

## Abbreviations

**α7 nAChR**
α7-homomeric nicotinic acetylcholine receptor

**BBB**
blood brain barrier

**BSA**
bovine serum albumin

**Cig**
cigarette-exposed mice

**DEG**
differentially expressed genes

**DI**
discrimination index

**EC0%**
nicotine-free e-cigarette exposed mice

**EC1.8%**
nicotine-containing e-cigarette exposed mice

**e-cigarettes, vaping**
electronic cigarettes

**e-liquid**
e-cigarette refill liquid

**EPM**
elevated plus maze

**FITC**
fluorescein isocyanate

**Glut1**
solute carrier family 2 (facilitated glucose transporter), member 1 (encoded by *Slc2a1*)

**Iba1**
ionized calcium binding adaptor molecule 1 (encoded by *Aif1*)

**icv**
intracerebroventricular

**LEL**
*Lycopersicon Esculentum* lectin

**NaF**
sodium fluorescein

**NORT**
novel object recognition test

**PG**
propylene glycol

**qPCR**
quantitative polymerase chain reaction

**ROI**
region of interest

**SAT**
spontaneous alternation task

**SE**
standard error of the mean

**smoking, cigarettes**
combustible tobacco cigarettes

**TJ**
tight junction

**TMR**
tetramethylrhodamine

**tpm**
total particulate matter

**VG**
vegetable glycerin

## 7. References

Abbott NJ, Patabendige AAK, Dolman DEM, Yusof SR, Begley DJ, 2010 Structure and function of the blood-brain barrier. Neurobiol. Dis 37, 13–25. 10.1016/j.nbd.2009.07.030 [PubMed: 19664713]

Abbruscato TJ, Lopez SP, Mark KS, Hawkins BT, Davis TP, 2002 Nicotine and cotinine modulate cerebral microvascular permeability and protein expression of ZO-1 through nicotinic acetylcholine receptors expressed on brain endothelial cells. J. Pharm. Sci 91, 2525–2538. 10.1002/jps.10256 [PubMed: 12434396]

Agaku IT, King BA, Husten CG, Bunnell R, Ambrose BK, Hu SS, Holder-Hayes E, Day HR, 2014 Tobacco Product Use Among Adults — United States, 2012–2013. MMWR Morb. Mortal. Wkly. Rep 63, 542–547. [PubMed: 24964880]

Alasmari F, Crotty Alexander LE, Hammad AM, Bojanowski CM, Moshensky A, Sari Y, 2019 Effects of Chronic Inhalation of Electronic Cigarette Vapor Containing Nicotine on Neurotransmitters in the Frontal Cortex and Striatum of C57BL/6 Mice. Front. Pharmacol 10, 885 10.3389/fphar.2019.00885 [PubMed: 31456684]

Alasmari F, Crotty Alexander LE, Nelson JA, Schiefer IT, Breen E, Drummond CA, Sari Y, 2017 Effects of chronic inhalation of electronic cigarettes containing nicotine on glial glutamate transporters and α-7 nicotinic acetylcholine receptor in female CD-1 mice. Prog. Neuropsychopharmacol. Biol. Psychiatry 77, 1–8. 10.1016/j.pnpbp.2017.03.017 [PubMed: 28347687]

An N, Andrukhov O, Tang Y, Falkensammer F, Bantleon H-P, Ouyang X, Rausch-Fan X, 2014 Effect of nicotine and porphyromonas gingivalis lipopolysaccharide on endothelial cells in vitro. PloS One 9, e96942 10.1371/journal.pone.0096942 [PubMed: 24820118]

Bahmed K, Lin C-R, Simborio H, Karim L, Aksoy M, Kelsen S, Tomar D, Madesh M, Elrod J, Messier E, Mason R, Unterwald EM, Eisenstein TK, Criner GJ, Kosmider B, 2019 The role of DJ-1 in human primary alveolar type II cell injury induced by e-cigarette aerosol. Am. J. Physiol. Lung Cell. Mol. Physiol 317, L475–L485. 10.1152/ajplung.00567.2018 [PubMed: 31313616]

Barber KE, Ghebrehiwet B, Yin W, Rubenstein DA, 2017 Endothelial Cell Inflammatory Reactions Are Altered in the Presence of E-Cigarette Extracts of Variable Nicotine. Cell. Mol. Bioeng 10, 124–133. 10.1007/s12195-016-0465-4 [PubMed: 31719854]

Barrington-Trimis JL, Leventhal AM, 2018 Adolescents' Use of "Pod Mod" E-Cigarettes - Urgent Concerns. N. Engl. J. Med 379, 1099–1102. 10.1056/NEJMp1805758 [PubMed: 30134127]

Bartalesi B, Cavarra E, Fineschi S, Lucattelli M, Lunghi B, Martorana PA, Lungarella G, 2005 Different lung responses to cigarette smoke in two strains of mice sensitive to oxidants. Eur. Respir. J 25, 15–22. 10.1183/09031936.04.00067204 [PubMed: 15640318]

Baumung C, Rehm J, Franke H, Lachenmeier DW, 2016 Comparative risk assessment of tobacco smoke constituents using the margin of exposure approach: the neglected contribution of nicotine. Sci. Rep 6, 35577 10.1038/srep35577 [PubMed: 27759090]

Beaglehole R, Bates C, Youdan B, Bonita R, 2019 Nicotine without smoke: fighting the tobacco epidemic with harm reduction. The Lancet 394, 718–720. 10.1016/S0140-6736(19)31884-7

Beauval N, Verrièle M, Garat A, Fronval I, Dusautoir R, Anthérieu S, Garçon G, Lo-Guidice J-M, Allorge D, Locoge N, 2019 Influence of puffing conditions on the carbonyl composition of e-cigarette aerosols. Int. J. Hyg. Environ. Health 222, 136–146. 10.1016/j.ijheh.2018.08.015 [PubMed: 30220464]

Bernstein DL, Zuluaga-Ramirez V, Gajghate S, Reichenbach NL, Polyak B, Persidsky Y, Rom S, 2019 miR-98 reduces endothelial dysfunction by protecting blood-brain barrier (BBB) and improves neurological outcomes in mouse ischemia/reperfusion stroke model. J. Cereb. Blood Flow Metab. Off. J. Int. Soc. Cereb. Blood Flow Metab 271678X19882264. 10.1177/0271678X19882264

Bold KW, Krishnan-Sarin S, 2019 E-cigarettes: Tobacco policy and regulation. Curr. Addict. Rep 6, 75–85. 10.1007/s40429-019-00243-5 [PubMed: 31555499]

Braber S, Henricks PAJ, Nijkamp FP, Kraneveld AD, Folkerts G, 2010 Inflammatory changes in the airways of mice caused by cigarette smoke exposure are only partially reversed after smoking cessation. Respir. Res 11, 99 10.1186/1465-9921-11-99 [PubMed: 20649997]

Brody AL, Gehlbach D, Garcia LY, Enoki R, Hoh C, Vera D, Kotta KK, London ED, Okita K, Nurmi EL, Seaman LC, Mandelkern MA, 2018 Effect of overnight smoking abstinence on a marker for microglial activation: a [11C]DAA1106 positron emission tomography study. Psychopharmacology (Berl.) 235, 3525–3534. 10.1007/s00213-018-5077-3 [PubMed: 30343364]

Brody AL, Hubert R, Enoki R, Garcia LY, Mamoun MS, Okita K, London ED, Nurmi EL, Seaman LC, Mandelkern MA, 2017 Effect of Cigarette Smoking on a Marker for Neuroinflammation: A [(11)C]DAA1106 Positron Emission Tomography Study. Neuropsychopharmacol. Off. Publ. Am. Coll. Neuropsychopharmacol 42, 1630–1639. 10.1038/npp.2017.48

Caporale A, Langham MC, Guo W, Johncola A, Chatterjee S, Wehrli FW, 2019 Acute Effects of Electronic Cigarette Aerosol Inhalation on Vascular Function Detected at Quantitative MRI. Radiology 293, 97–106. 10.1148/radiol.2019190562 [PubMed: 31429679]

Cataldo JK, Prochaska JJ, Glantz SA, 2010 Cigarette smoking is a risk factor for Alzheimer's Disease: an analysis controlling for tobacco industry affiliation. J. Alzheimers Dis. JAD 19, 465–480. 10.3233/JAD-2010-1240 [PubMed: 20110594]

Chae C, Walters MJ, Holman MR, 2017 International Organization of Standardization (ISO) and Cambridge Filter Test (CFT) Smoking Regimen Data Comparisons in Tobacco Product Marketing Applications. Tob. Regul. Sci 3, 258–265. 10.18001/TRS.3.3.2 [PubMed: 28798947]

Chaumont M, de Becker B, Zaher W, Culié A, Deprez G, Mélot C, Reyé F, Van Antwerpen P, Delporte C, Debbas N, Boudjeltia KZ, van de Borne P, 2018 Differential Effects of E-Cigarette on Microvascular Endothelial Function, Arterial Stiffness and Oxidative Stress: A Randomized Crossover Trial. Sci. Rep 8, 10378 10.1038/s41598-018-28723-0 [PubMed: 29991814]

Chen H, Cowan MJ, Hasday JD, Vogel SN, Medvedev AE, 2007 Tobacco smoking inhibits expression of proinflammatory cytokines and activation of IL-1R-associated kinase, p38, and NF-kappaB in alveolar macrophages stimulated with TLR2 and TLR4 agonists. J. Immunol. Baltim. Md 1950 179, 6097–6106. 10.4049/jimmunol.179.9.6097

Cummins PM, 2012 Occludin: One Protein, Many Forms. Mol. Cell. Biol 32, 242–250. 10.1128/MCB.06029-11 [PubMed: 22083955]

Dawkins LE, Kimber CF, Doig M, Feyerabend C, Corcoran O, 2016 Self-titration by experienced e-cigarette users: blood nicotine delivery and subjective effects. Psychopharmacology (Berl.) 233, 2933–2941. 10.1007/s00213-016-4338-2 [PubMed: 27235016]

Duell AK, McWhirter KJ, Korzun T, Strongin RM, Peyton DH, 2019 Sucralose-Enhanced Degradation of Electronic Cigarette Liquids during Vaping. Chem. Res. Toxicol 32, 1241–1249. 10.1021/acs.chemrestox.9b00047 [PubMed: 31079450]

El-Mas MM, El-Gowelli HM, El-Gowilly SM, Fouda MA, Helmy MM, 2012 Estrogen provokes the depressant effect of chronic nicotine on vagally mediated reflex chronotropism in female rats. J. Pharmacol. Exp. Ther 342, 568–575. 10.1124/jpet.112.191940 [PubMed: 22619254]

Erythropel HC, Jabba SV, DeWinter TM, Mendizabal M, Anastas PT, Jordt SE, Zimmerman JB, 2019 Formation of flavorant-propylene Glycol Adducts With Novel Toxicological Properties in Chemically Unstable E-Cigarette Liquids. Nicotine Tob. Res. Off. J. Soc. Res. Nicotine Tob 21, 1248–1258. 10.1093/ntr/nty192

Etter J-F, 2016 A longitudinal study of cotinine in long-term daily users of e-cigarettes. Drug Alcohol Depend 160, 218–221. 10.1016/j.drugalcdep.2016.01.003 [PubMed: 26804899]

Farsalinos KE, Gillman G, 2017 Carbonyl Emissions in E-cigarette Aerosol: A Systematic Review and Methodological Considerations. Front. Physiol 8, 1119 10.3389/fphys.2017.01119 [PubMed: 29375395]

Farsalinos KE, Voudris V, Poulas K, 2015 E-cigarettes generate high levels of aldehydes only in "dry puff" conditions. Addict. Abingdon Engl 110, 1352–1356. 10.1111/add.12942

Franzen KF, Willig J, Cayo Talavera S, Meusel M, Sayk F, Reppel M, Dalhoff K, Mortensen K, Droemann D, 2018 E-cigarettes and cigarettes worsen peripheral and central hemodynamics as well as arterial stiffness: A randomized, double-blinded pilot study. Vasc. Med. Lond. Engl 23, 419–425. 10.1177/1358863X18779694

Gentzke AS, Creamer M, Cullen KA, Ambrose BK, Willis G, Jamal A, King BA, 2019 Vital Signs: Tobacco Product Use Among Middle and High School Students - United States, 2011–2018. MMWR Morb. Mortal. Wkly. Rep 68, 157–164. 10.15585/mmwr.mm6806e1 [PubMed: 30763302]

Glynos C, Bibli S-I, Katsaounou P, Pavlidou A, Magkou C, Karavana V, Topouzis S, Kalomenidis I, Zakynthinos S, Papapetropoulos A, 2018 Comparison of the effects of e-cigarette vapor with cigarette smoke on lung function and inflammation in mice. Am. J. Physiol. Lung Cell. Mol. Physiol 315, L662–L672. 10.1152/ajplung.00389.2017 [PubMed: 30091379]

Goniewicz ML, Boykan R, Messina CR, Eliscu A, Tolentino J, 2019 High exposure to nicotine among adolescents who use Juul and other vape pod systems ('pods'). Tob. Control 28, 676–677. 10.1136/tobaccocontrol-2018-054565 [PubMed: 30194085]

Goniewicz ML, Gawron M, Smith DM, Peng M, Jacob P, Benowitz NL, 2017 Exposure to Nicotine and Selected Toxicants in Cigarette Smokers Who Switched to Electronic Cigarettes: A

Longitudinal Within-Subjects Observational Study. Nicotine Tob. Res. Off. J. Soc. Res. Nicotine Tob 19, 160–167. 10.1093/ntr/ntw160

Hage AN, Krause W, Mathues A, Krasner L, Kasten S, Eliason JL, Ghosh A, 2017 Comparing the Effects of Electronic Cigarette Vapor and Cigarette Smoke in a Novel In Vivo Exposure System. J. Vis. Exp. JoVE 10.3791/55672

Hashimoto K, Zaima N, Sekiguchi H, Kugo H, Miyamoto C, Hoshino K, Kawasaki N, Sutoh K, Usumi K, Moriyama T, 2018 Dietary DNA Attenuates the Degradation of Elastin Fibers in the Aortic Wall in Nicotine-Administrated Mice. J. Nutr. Sci. Vitaminol. (Tokyo) 64, 271–276. 10.3177/jnsv.64.271 [PubMed: 30175790]

Haussmann H-J, 2012 Use of hazard indices for a theoretical evaluation of cigarette smoke composition. Chem. Res. Toxicol 25, 794–810. 10.1021/tx200536w [PubMed: 22352345]

Hawkins BT, Abbruscato TJ, Egleton RD, Brown RC, Huber JD, Campos CR, Davis TP, 2004 Nicotine increases in vivo blood-brain barrier permeability and alters cerebral microvascular tight junction protein distribution. Brain Res 1027, 48–58. 10.1016/j.brainres.2004.08.043 [PubMed: 15494156]

Hawkins BT, Egleton RD, Davis TP, 2005 Modulation of cerebral microvascular permeability by endothelial nicotinic acetylcholine receptors. Am. J. Physiol. Heart Circ. Physiol 289, H212–219. 10.1152/ajpheart.01210.2004 [PubMed: 15708958]

Hecht SS, Carmella SG, Kotandeniya D, Pillsbury ME, Chen M, Ransom BWS, Vogel RI, Thompson E, Murphy SE, Hatsukami DK, 2015 Evaluation of toxicant and carcinogen metabolites in the urine of e-cigarette users versus cigarette smokers. Nicotine Tob. Res. Off. J. Soc. Res. Nicotine Tob 17, 704–709. 10.1093/ntr/ntu218

Holliday ED, Nucero P, Kutlu MG, Oliver C, Connelly KL, Gould TJ, Unterwald EM, 2016 Long-term effects of chronic nicotine on emotional and cognitive behaviors and hippocampus cell morphology in mice: comparisons of adult and adolescent nicotine exposure. Eur. J. Neurosci 44, 2818–2828. 10.1111/ejn.13398 [PubMed: 27623427]

Hukkanen J, Jacob P, Benowitz NL, 2005 Metabolism and disposition kinetics of nicotine. Pharmacol. Rev 57, 79–115. 10.1124/pr.57.1.3 [PubMed: 15734728]

Jeelani R, Khan SN, Shaeib F, Kohan-Ghadr H-R, Aldhaheri SR, Najafi T, Thakur M, Morris R, Abu-Soud HM, 2017 Cyclophosphamide and acrolein induced oxidative stress leading to deterioration of metaphase II mouse oocyte quality. Free Radic. Biol. Med 110, 11–18. 10.1016/j.freeradbiomed.2017.05.006 [PubMed: 28499912]

Jensen RP, Luo W, Pankow JF, Strongin RM, Peyton DH, 2015 Hidden formaldehyde in e-cigarette aerosols. N. Engl. J. Med 372, 392–394. 10.1056/NEJMc1413069 [PubMed: 25607446]

Kann L, McManus T, Harris WA, Shanklin SL, Flint KH, Queen B, Lowry R, Chyen D, Whittle L, Thornton J, Lim C, Bradford D, Yamakawa Y, Leon M, Brener N, Ethier KA, 2018 Youth Risk Behavior Surveillance - United States, 2017. Morb. Mortal. Wkly. Rep. Surveill. Summ. Wash. DC 2002 67, 1–114. 10.15585/mmwr.ss6708a1

Keith RJ, Fetterman JL, Orimoloye OA, Dardari Z, Lorkiewicz P, Hamburg NM, DeFilippis AP, Blaha MJ, Bhatnagar A, 2019 Characterization of Volatile Organic Compound (VOC) metabolites in Cigarette smokers, Electronic Nicotine Device Users, Dual Users and Non- users of tobacco. Nicotine Tob. Res. Off. J. Soc. Res. Nicotine Tob 10.1093/ntr/ntz021

Kraeuter A-K, Guest PC, Sarnyai Z, 2019 The Y-Maze for Assessment of Spatial Working and Reference Memory in Mice. Methods Mol. Biol. Clifton NJ 1916, 105–111. 10.1007/978-1-4939-8994-2_10

Krafft PR, Caner B, Klebe D, Rolland WB, Tang J, Zhang JH, 2013 PHA-543613 preserves blood-brain barrier integrity after intracerebral hemorrhage in mice. Stroke 44, 1743–1747. 10.1161/STROKEAHA.111.000427 [PubMed: 23613493]

Kuntic M, Oelze M, Steven S, Kröller-Schön S, Stamm P, Kalinovic S, Frenis K, Vujacic-Mirski K, Bayo Jimenez MT, Kvandova M, Filippou K, Al Zuabi A, Brückl V, Hahad O, Daub S, Varveri F, Gori T, Huesmann R, Hoffmann T, Schmidt FP, Keaney JF, Daiber A, Münzel T, 2019 Short-term e-cigarette vapour exposure causes vascular oxidative stress and dysfunction: evidence for a close connection to brain damage and a key role of the phagocytic NADPH oxidase (NOX-2). Eur. Heart J 10.1093/eurheartj/ehz772

Kuwabara H, Kokai Y, Kojima T, Takakuwa R, Mori M, Sawada N, 2001 Occludin regulates actin cytoskeleton in endothelial cells. Cell Struct. Funct 26, 109–116. 10.1247/csf.26.109 [PubMed: 11482453]

Landry RL, Groom AL, Vu T-HT, Stokes AC, Berry KM, Kesh A, Hart JL, Walker KL, Giachello AL, Sears CG, McGlasson KL, Tompkins LK, Mattingly DT, Robertson RM, Payne TJ, 2019 The role of flavors in vaping initiation and satisfaction among U.S. adults. Addict. Behav 99, 106077 10.1016/j.addbeh.2019.106077 [PubMed: 31437770]

Larcombe AN, Janka MA, Mullins BJ, Berry LJ, Bredin A, Franklin PJ, 2017 The effects of electronic cigarette aerosol exposure on inflammation and lung function in mice. Am. J. Physiol. Lung Cell. Mol. Physiol 313, L67–L79. 10.1152/ajplung.00203.2016 [PubMed: 28360111]

Lariscy JT, 2019 Smoking-attributable mortality by cause of death in the United States: An indirect approach. SSM - Popul. Health 7 10.1016/j.ssmph.2019.100349

Lee KM, Hoeng J, Harbo S, Kogel U, Gardner W, Oldham M, Benson E, Talikka M, Kondylis A, Martin F, Titz B, Ansari S, Trivedi K, Guedj E, Elamin A, Ivanov NV, Vanscheeuwijck P, Peitsch MC, McKinney WJ, 2018 Biological changes in C57BL/6 mice following 3 weeks of inhalation exposure to cigarette smoke or e-vapor aerosols. Inhal. Toxicol 30, 553–567. 10.1080/08958378.2019.1576807 [PubMed: 30849254]

Lee Y-K, Uchida H, Smith H, Ito A, Sanchez T, 2019 The isolation and molecular characterization of cerebral microvessels. Nat. Protoc 10.1038/s41596-019-0212-0

Lerner CA, Sundar IK, Yao H, Gerloff J, Ossip DJ, McIntosh S, Robinson R, Rahman I, 2015 Vapors produced by electronic cigarettes and e-juices with flavorings induce toxicity, oxidative stress, and inflammatory response in lung epithelial cells and in mouse lung. PloS One 10, e0116732 10.1371/journal.pone.0116732 [PubMed: 25658421]

Li X, Han X, Bao J, Liu Y, Ye A, Thakur M, Liu H, 2016 Nicotine increases eclampsia-like seizure threshold and attenuates microglial activity in rat hippocampus through the α7 nicotinic acetylcholine receptor. Brain Res 1642, 487–496. 10.1016/j.brainres.2016.04.043 [PubMed: 27106269]

Marks MJ, Burch JB, Collins AC, 1983 Genetics of nicotine response in four inbred strains of mice. J. Pharmacol. Exp. Ther 226, 291–302. [PubMed: 6864548]

Marsot A, Simon N, 2016 Nicotine and Cotinine Levels With Electronic Cigarette: A Review. Int. J. Toxicol 35, 179–185. 10.1177/1091581815618935 [PubMed: 26681385]

McRobbie H, Phillips A, Goniewicz ML, Smith KM, Knight-West O, Przulj D, Hajek P, 2015 Effects of Switching to Electronic Cigarettes with and without Concurrent Smoking on Exposure to Nicotine, Carbon Monoxide, and Acrolein. Cancer Prev. Res. Phila. Pa 8, 873–878. 10.1158/1940-6207.CAPR-15-0058

Middlekauff HR, Park J, Agrawal H, Gornbein JA, 2013 Abnormal sympathetic nerve activity in women exposed to cigarette smoke: a potential mechanism to explain increased cardiac risk. Am. J. Physiol. Heart Circ. Physiol 305, H1560–1567. 10.1152/ajpheart.00502.2013 [PubMed: 23997107]

Munji RN, Soung AL, Weiner GA, Sohet F, Semple BD, Trivedi A, Gimlin K, Kotoda M, Korai M, Aydin S, Batugal A, Cabangcala AC, Schupp PG, Oldham MC, Hashimoto T, Noble-Haeusslein LJ, Daneman R, 2019 Profiling the mouse brain endothelial transcriptome in health and disease models reveals a core blood-brain barrier dysfunction module. Nat. Neurosci 10.1038/s41593-019-0497-x

Nardone N, Helen GS, Addo N, Meighan S, Benowitz NL, 2019 JUUL electronic cigarettes: Nicotine exposure and the user experience. Drug Alcohol Depend 203, 83–87. 10.1016/j.drugalcdep.2019.05.019 [PubMed: 31408770]

Nation DA, Sweeney MD, Montagne A, Sagare AP, D'Orazio LM, Pachicano M, Sepehrband F, Nelson AR, Buennagel DP, Harrington MG, Benzinger TLS, Fagan AM, Ringman JM, Schneider LS, Morris JC, Chui HC, Law M, Toga AW, Zlokovic BV, 2019 Blood-brain barrier breakdown is an early biomarker of human cognitive dysfunction. Nat. Med 25, 270–276. 10.1038/s41591-018-0297-y [PubMed: 30643288]

O'Donnell MJ, Chin SL, Rangarajan S, Xavier D, Liu L, Zhang H, Rao-Melacini P, Zhang X, Pais P, Agapay S, Lopez-Jaramillo P, Damasceno A, Langhorne P, McQueen MJ, Rosengren A, Dehghan M, Hankey GJ, Dans AL, Elsayed A, Avezum A, Mondo C, Diener H-C, Ryglewicz D,

Czlonkowska A, Pogosova N, Weimar C, Iqbal R, Diaz R, Yusoff K, Yusufali A, Oguz A, Wang X, Penaherrera E, Lanas F, Ogah OS, Ogunniyi A, Iversen HK, Malaga G, Rumboldt Z, Oveisgharan S, Al Hussain F, Magazi D, Nilanont Y, Ferguson J, Pare G, Yusuf S, INTERSTROKE investigators, 2016 Global and regional effects of potentially modifiable risk factors associated with acute stroke in 32 countries (INTERSTROKE): a case-control study. Lancet Lond. Engl 388, 761–775. 10.1016/S0140-6736(16)30506-2

Olfert IM, DeVallance E, Hoskinson H, Branyan KW, Clayton S, Pitzer CR, Sullivan DP, Breit MJ, Wu Z, Klinkhachorn P, Mandler WK, Erdreich BH, Ducatman BS, Bryner RW, Dasgupta P, Chantler PD, 2018 Chronic exposure to electronic cigarettes results in impaired cardiovascular function in mice. J. Appl. Physiol. Bethesda Md 1985 124, 573–582. 10.1152/japplphysiol.00713.2017

Persidsky Y, Heilman D, Haorah J, Zelivyanskaya M, Persidsky R, Weber GA, Shimokawa H, Kaibuchi K, Ikezu T, 2006 Rho-mediated regulation of tight junctions during monocyte migration across the blood-brain barrier in HIV-1 encephalitis (HIVE). Blood 107, 4770–4780. 10.1182/blood-2005-11-4721 [PubMed: 16478881]

Prasad S, Sajja RK, Kaisar MA, Park JH, Villalba H, Liles T, Abbruscato T, Cucullo L, 2017 Role of Nrf2 and protective effects of Metformin against tobacco smoke-induced cerebrovascular toxicity. Redox Biol 12, 58–69. 10.1016/j.redox.2017.02.007 [PubMed: 28212524]

Reilly SM, Bitzer ZT, Goel R, Trushin N, Richie JP, 2019 Free Radical, Carbonyl, and Nicotine Levels Produced by Juul Electronic Cigarettes. Nicotine Tob. Res. Off. J. Soc. Res. Nicotine Tob 21, 1274–1278. 10.1093/ntr/nty221

Revathikumar P, Bergqvist F, Gopalakrishnan S, Korotkova M, Jakobsson P-J, Lampa J, Le Maître E, 2016 Immunomodulatory effects of nicotine on interleukin 1β activated human astrocytes and the role of cyclooxygenase 2 in the underlying mechanism. J. Neuroinflammation 13, 256 10.1186/s12974-016-0725-1 [PubMed: 27681882]

Rom S, Dykstra H, Zuluaga-Ramirez V, Reichenbach NL, Persidsky Y, 2015a miR-98 and let-7g* protect the blood-brain barrier under neuroinflammatory conditions. J. Cereb. Blood Flow Metab. Off. J. Int. Soc. Cereb. Blood Flow Metab 35, 1957–1965. 10.1038/jcbfm.2015.154

Rom S, Reichenbach NL, Dykstra H, Persidsky Y, 2015b The dual action of poly(ADP-ribose) polymerase -1 (PARP-1) inhibition in HIV-1 infection: HIV-1 LTR inhibition and diminution in Rho GTPase activity. Front. Microbiol 6, 878 10.3389/fmicb.2015.00878 [PubMed: 26379653]

Rom S, Zuluaga-Ramirez V, Gajghate S, Seliga A, Winfield M, Heldt NA, Kolpakov MA, Bashkirova YV, Sabri AK, Persidsky Y, 2019 Hyperglycemia-Driven Neuroinflammation Compromises BBB Leading to Memory Loss in Both Diabetes Mellitus (DM) Type 1 and Type 2 Mouse Models. Mol. Neurobiol 56, 1883–1896. 10.1007/s12035-018-1195-5 [PubMed: 29974394]

Romberg AR, Miller Lo EJ, Cuccia AF, Willett JG, Xiao H, Hair EC, Vallone DM, Marynak K, King BA, 2019 Patterns of nicotine concentrations in electronic cigarettes sold in the United States, 2013–2018. Drug Alcohol Depend 203, 1–7. 10.1016/j.drugalcdep.2019.05.029 [PubMed: 31386973]

Rubenstein DA, Hom S, Ghebrehiwet B, Yin W, 2015 Tobacco and e-cigarette products initiate Kupffer cell inflammatory responses. Mol. Immunol 67, 652–660. 10.1016/j.molimm.2015.05.020 [PubMed: 26072673]

Saiki R, Hayashi D, Ikuo Y, Nishimura K, Ishii I, Kobayashi K, Chiba K, Toida T, Kashiwagi K, Igarashi K, 2013 Acrolein stimulates the synthesis of IL-6 and C-reactive protein (CRP) in thrombosis model mice and cultured cells. J. Neurochem 127, 652–659. 10.1111/jnc.12336 [PubMed: 23763486]

Saitou M, Furuse M, Sasaki H, Schulzke J-D, Fromm M, Takano H, Noda T, Tsukita S, 2000 Complex Phenotype of Mice Lacking Occludin, a Component of Tight Junction Strands. Mol. Biol. Cell 11, 4131–4142. [PubMed: 11102513]

Saravia R, Ten-Blanco M, Grande MT, Maldonado R, Berrendero F, 2019 Anti-inflammatory agents for smoking cessation? Focus on cognitive deficits associated with nicotine withdrawal in male mice. Brain. Behav. Immun 75, 228–239. 10.1016/j.bbi.2018.11.003 [PubMed: 30391635]

Schick SF, Blount BC, Jacob P, Saliba NA, Bernert JT, El Hellani A, Jatlow P, Pappas RS, Wang L, Foulds J, Ghosh A, Hecht SS, Gomez JC, Martin JR, Mesaros C, Srivastava S, St Helen G, Tarran R, Lorkiewicz PK, Blair IA, Kimmel HL, Doerschuk CM, Benowitz NL, Bhatnagar A, 2017

Biomarkers of exposure to new and emerging tobacco delivery products. Am. J. Physiol. Lung Cell. Mol. Physiol 313, L425–L452. 10.1152/ajplung.00343.2016 [PubMed: 28522563]

Schweitzer KS, Chen SX, Law S, Van Demark M, Poirier C, Justice MJ, Hubbard WC, Kim ES, Lai X, Wang M, Kranz WD, Carroll CJ, Ray BD, Bittman R, Goodpaster J, Petrache I, 2015 Endothelial disruptive proinflammatory effects of nicotine and e-cigarette vapor exposures. Am. J. Physiol. Lung Cell. Mol. Physiol 309, L175–187. 10.1152/ajplung.00411.2014 [PubMed: 25979079]

Sharentuya N, Tomimatsu T, Mimura K, Tskitishvili E, Kinugasa-Taniguchi Y, Kanagawa T, Kimura T, 2010 Nicotine suppresses interleukin-6 production from vascular endothelial cells: a possible therapeutic role of nicotine for preeclampsia. Reprod. Sci. Thousand Oaks Calif 17, 556–563. 10.1177/1933719110362594

Shi H, Fan X, Horton A, Haller ST, Kennedy DJ, Schiefer IT, Dworkin L, Cooper CJ, Tian J, 2019 The Effect of Electronic-Cigarette Vaping on Cardiac Function and Angiogenesis in Mice. Sci. Rep 9, 4085 10.1038/s41598-019-40847-5 [PubMed: 30858470]

Shi X, Barr JL, von Weltin E, Wolsh C, Unterwald EM, 2019 Differential Roles of Accumbal GSK3β in Cocaine versus Morphine-Induced Place Preference, U50,488H-Induced Place Aversion, and Object Memory. J. Pharmacol. Exp. Ther 371, 339–347. 10.1124/jpet.119.259283 [PubMed: 31420527]

Siu ECK, Tyndale RF, 2007 Characterization and comparison of nicotine and cotinine metabolism in vitro and in vivo in DBA/2 and C57BL/6 mice. Mol. Pharmacol 71, 826–834. 10.1124/mol.106.032086 [PubMed: 17158199]

Sleiman M, Logue JM, Montesinos VN, Russell ML, Litter MI, Gundel LA, Destaillats H, 2016 Emissions from Electronic Cigarettes: Key Parameters Affecting the Release of Harmful Chemicals. Environ. Sci. Technol 50, 9644–9651. 10.1021/acs.est.6b01741 [PubMed: 27461870]

Soneji S, Barrington-Trimis JL, Wills TA, Leventhal AM, Unger JB, Gibson LA, Yang J, Primack BA, Andrews JA, Miech RA, Spindle TR, Dick DM, Eissenberg T, Hornik RC, Dang R, Sargent JD, 2017 Association Between Initial Use of e-Cigarettes and Subsequent Cigarette Smoking Among Adolescents and Young Adults: A Systematic Review and Meta-analysis. JAMA Pediatr 171, 788–797. 10.1001/jamapediatrics.2017.1488 [PubMed: 28654986]

Stallings-Smith S, Ballantyne T, 2019 Ever Use of E-Cigarettes Among Adults in the United States: A Cross-Sectional Study of Sociodemographic Factors. Inq. J. Med. Care Organ. Provis. Financ 56, 46958019864479 10.1177/0046958019864479

Stone E, Marshall H, 2019 Electronic cigarettes in physician practice: a complex debate. Intern. Med. J 49, 438–445. 10.1111/imj.14256 [PubMed: 30957372]

Sussan TE, Gajghate S, Thimmulappa RK, Ma J, Kim J-H, Sudini K, Consolini N, Cormier SA, Lomnicki S, Hasan F, Pekosz A, Biswal S, 2015 Exposure to electronic cigarettes impairs pulmonary anti-bacterial and anti-viral defenses in a mouse model. PloS One 10, e0116861 10.1371/journal.pone.0116861 [PubMed: 25651083]

Sweeney MD, Kisler K, Montagne A, Toga AW, Zlokovic BV, 2018 The role of brain vasculature in neurodegenerative disorders. Nat. Neurosci 21, 1318–1331. 10.1038/s41593-018-0234-x [PubMed: 30250261]

Talih S, Salman R, Karaoghlanian N, El-Hellani A, Saliba N, Eissenberg T, Shihadeh A, 2017 “Juice Monsters”: Sub-Ohm Vaping and Toxic Volatile Aldehyde Emissions. Chem. Res. Toxicol 30, 1791–1793. 10.1021/acs.chemrestox.7b00212 [PubMed: 28937746]

Toth P, Tarantini S, Csiszar A, Ungvari Z, 2017 Functional vascular contributions to cognitive impairment and dementia: mechanisms and consequences of cerebral autoregulatory dysfunction, endothelial impairment, and neurovascular uncoupling in aging. Am. J. Physiol. Heart Circ. Physiol 312, H1–H20. 10.1152/ajpheart.00581.2016 [PubMed: 27793855]

Tsuji H, Fujimoto H, Matsuura D, Nishino T, Lee KM, Renne R, Yoshimura H, 2011 Comparison of mouse strains and exposure conditions in acute cigarette smoke inhalation studies. Inhal. Toxicol 23, 602–615. 10.3109/08958378.2011.596851 [PubMed: 21864220]

Ueno H, Pradhan S, Schlessel D, Hirasawa H, Sumpio BE, 2006 Nicotine enhances human vascular endothelial cell expression of ICAM-1 and VCAM-1 via protein kinase C, p38 mitogen-activated protein kinase, NF-kappaB, and AP-1. Cardiovasc. Toxicol 6, 39–50. [PubMed: 16845181]

van Dijk EJ, Prins ND, Vrooman HA, Hofman A, Koudstaal PJ, Breteler MMB, 2008 Progression of cerebral small vessel disease in relation to risk factors and cognitive consequences: Rotterdam Scan study. Stroke 39, 2712–2719. 10.1161/STROKEAHA.107.513176 [PubMed: 18635849]

Villaseñor R, Kuennecke B, Ozmen L, Ammann M, Kugler C, Grüninger F, Loetscher H, Freskgård P-O, Collin L, 2017 Region-specific permeability of the blood-brain barrier upon pericyte loss. J. Cereb. Blood Flow Metab. Off. J. Int. Soc. Cereb. Blood Flow Metab 37, 3683–3694. 10.1177/0271678X17697340

Wagener TL, Floyd EL, Stepanov I, Driskill LM, Frank SG, Meier E, Leavens EL, Tackett AP, Molina N, Queimado L, 2017 Have combustible cigarettes met their match? The nicotine delivery profiles and harmful constituent exposures of second-generation and third-generation electronic cigarette users. Tob. Control 26, e23–e28. 10.1136/tobaccocontrol-2016-053041 [PubMed: 27729564]

Wagenhäuser MU, Schellinger IN, Yoshino T, Toyama K, Kayama Y, Deng A, Guenther SP, Petzold A, Mulorz J, Mulorz P, Hasenfuß G, Ibing W, Elvers M, Schuster A, Ramasubramanian AK, Adam M, Schelzig H, Spin JM, Raaz U, Tsao PS, 2018 Chronic Nicotine Exposure Induces Murine Aortic Remodeling and Stiffness Segmentation-Implications for Abdominal Aortic Aneurysm Susceptibility. Front. Physiol 9, 1459 10.3389/fphys.2018.01459 [PubMed: 30429794]

Yasuda M, Ota T, Morikawa A, Mawatari K, Fukuuchi T, Yamaoka N, Kaneko K, Nakagomi K, 2013 Simultaneous determination of nicotine and cotinine in serum using high-performance liquid chromatography with fluorometric detection and postcolumn UV-photoirradiation system. J. Chromatogr. B Analyt. Technol. Biomed. Life. Sci 934, 41–45. 10.1016/j.jchromb.2013.06.028

Yoshida M, Tomitori H, Machi Y, Hagihara M, Higashi K, Goda H, Ohya T, Niitsu M, Kashiwagi K, Igarashi K, 2009a Acrolein toxicity: Comparison with reactive oxygen species. Biochem. Biophys. Res. Commun. 378, 313–318. 10.1016/j.bbrc.2008.11.054 [PubMed: 19032949]

Yoshida M, Tomitori H, Machi Y, Katagiri D, Ueda S, Horiguchi K, Kobayashi E, Saeki N, Nishimura K, Ishii I, Kashiwagi K, Igarashi K, 2009b Acrolein, IL-6 and CRP as markers of silent brain infarction. Atherosclerosis 203, 557–562. 10.1016/j.atherosclerosis.2008.07.022 [PubMed: 18757054]

Yun JH, Morrow J, Owen CA, Qiu W, Glass K, Lao T, Jiang Z, Perrella MA, Silverman EK, Zhou X, Hersh CP, 2017 Transcriptomic Analysis of Lung Tissue from Cigarette Smoke–Induced Emphysema Murine Models and Human Chronic Obstructive Pulmonary Disease Show Shared and Distinct Pathways. Am. J. Respir. Cell Mol. Biol 57, 47–58. 10.1165/rcmb.2016-0328OC [PubMed: 28248572]

Zelikoff JT, Parmalee NL, Corbett K, Gordon T, Klein CB, Aschner M, 2018 Microglia Activation and Gene Expression Alteration of Neurotrophins in the Hippocampus Following Early-Life Exposure to E-Cigarette Aerosols in a Murine Model. Toxicol. Sci. Off. J. Soc. Toxicol 162, 276–286. 10.1093/toxsci/kfx257

Zuluaga-Ramirez V, Rom S, Persidsky Y, 2015 Craniula: A cranial window technique for prolonged imaging of brain surface vasculature with simultaneous adjacent intracerebral injection. Fluids Barriers CNS 12, 24 10.1186/s12987-015-0021-y [PubMed: 26507826]

## Highlights

- Electronic cigarettes reduce expression of Occludin in limbic brain regions
- TNF-induced leukocyte adhesion to brain endothelium is worsened by electronic cigarettes
- Nicotine-free electronic cigarettes worsen novel object recognition performance

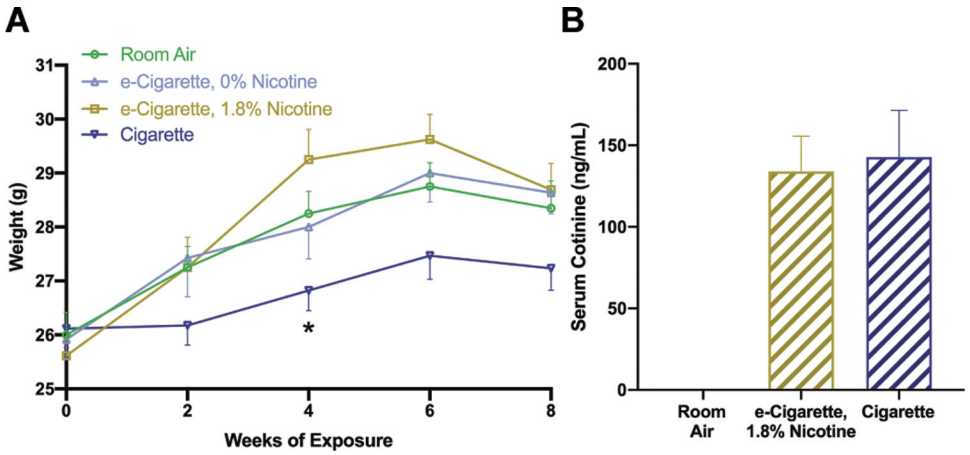


**Figure 1.**

Inhalation exposure of mice to e-cigarettes or cigarettes mimics body weight and biomarker trends in human users. Weights were assessed (A) at 2-week intervals prior to the daily exposure period. Whole blood was collected 1 hour following the daily exposure period and assessed by LC-MS/MS for cotinine (B) as a marker for intake of nicotine-containing products. Data are expressed as group mean ± standard error. *, $p < 0.05$ versus room air. Two-way ANOVA was applied to weights [exposure, $F(3,47)=6.310$, $p=0.0011$; time, $F(1,47)=0.0249$, $p=0.0249$); interaction, $F(3,47)=0.8543$, $p=0.4714$] and *Student's* t-test applied across cotinine measurements of EC1.8% and Cig groups [$t(32)=0.2275$, $p=0.8215$]. n = 20 mice/group.

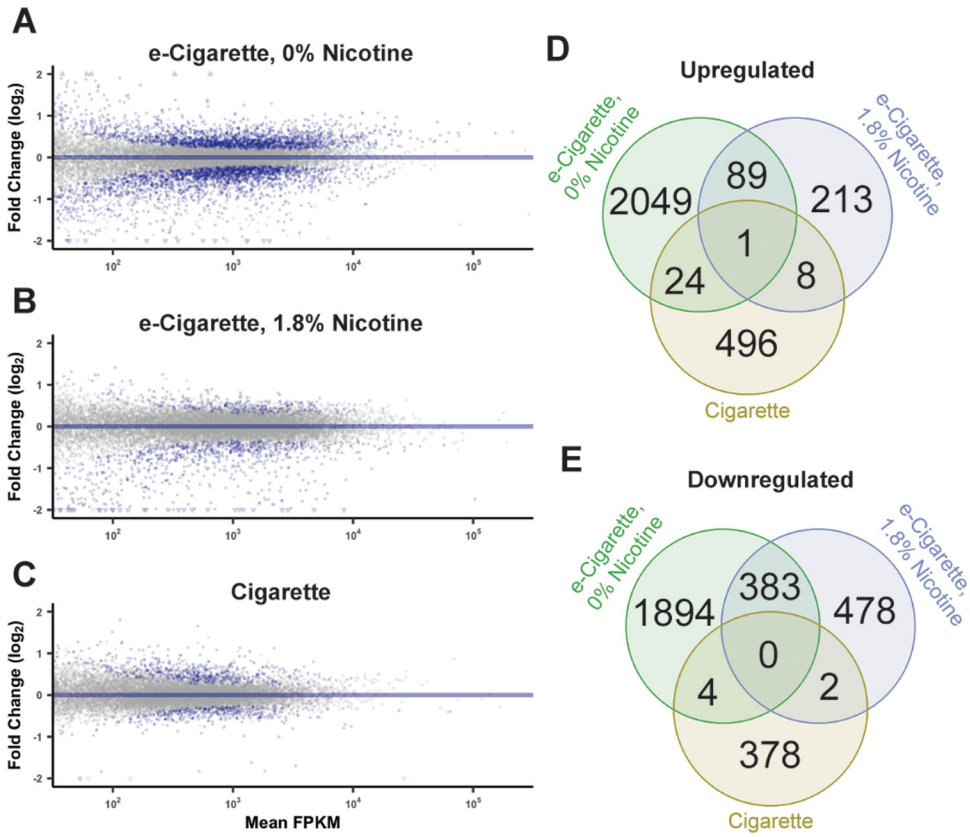


**Figure 2.**

E-cigarette and cigarette exposure have a unique transcriptional profile within cerebral microvessels. mRNA was isolated from isolated cerebral microvessels and sequenced for detection of differentially expressed genes (DEG) (n = 3–4 mice/group). Plots of fold change from room air ($log_2$ scale) versus mean fragments per kilobase of transcript per million (FPKM) are shown for each treatment group (A-C). Transcripts which were up- or downregulated to a statistically significant extent are shown in blue with all others shown in grey. Arrowheads indicated transcripts with fold change above or below the shown axes. Total quantity of upregulated (D) or downregulated (E) DEG is indicated for each exposure group, and are further subdivided into genes which are uniquely changed versus those that are shared across multiple exposure groups on the respective Venn diagram. Statistical significance was determined using a negative binomial generalized linear model with Benjamini-Hochberg multiple comparison correction.

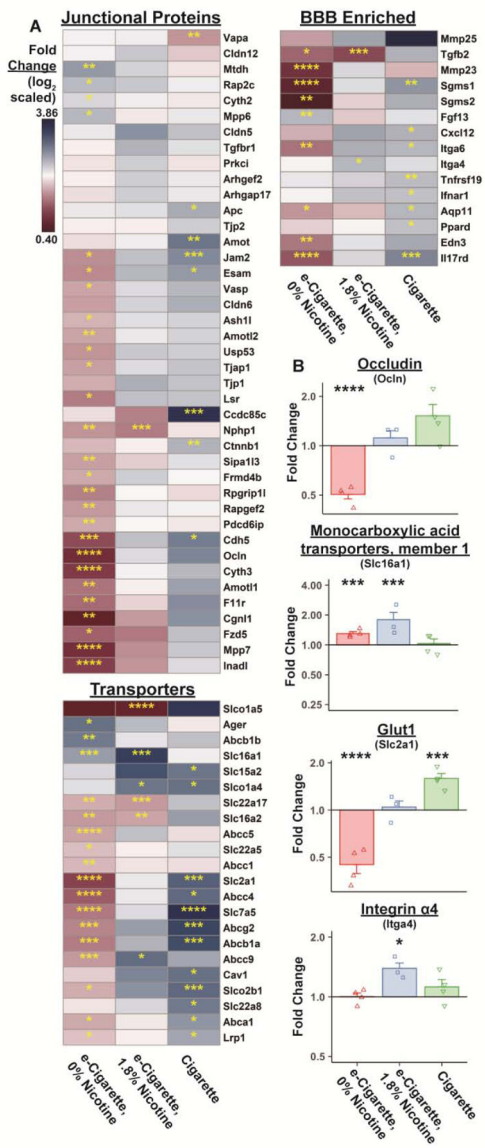


**Figure 3.**

mRNA expression of tight junction-, transport-, and immune-related genes is dysregulated following exposure to e-cigarettes or cigarettes. Mean gene expression relative to room air is indicated for each group using a $\log_2$ scale for DEGs with a known role at the BBB (A). DEGs have been functionally divided into groups which are either localized at tight junctions, play a role in drug efflux or nutrient transport, or have immune-related roles. Fold change for selected genes from these groups are shown in (B) using the RNA-seq dataset. Fold change per individual animal is indicated by points (n = 3–4 mice/group). Group mean and standard error are indicated by bars. *, $p < 0.05$; **, $p < 0.01$; ***, $p < 0.001$; ****, $p < 0.0001$ versus room air.

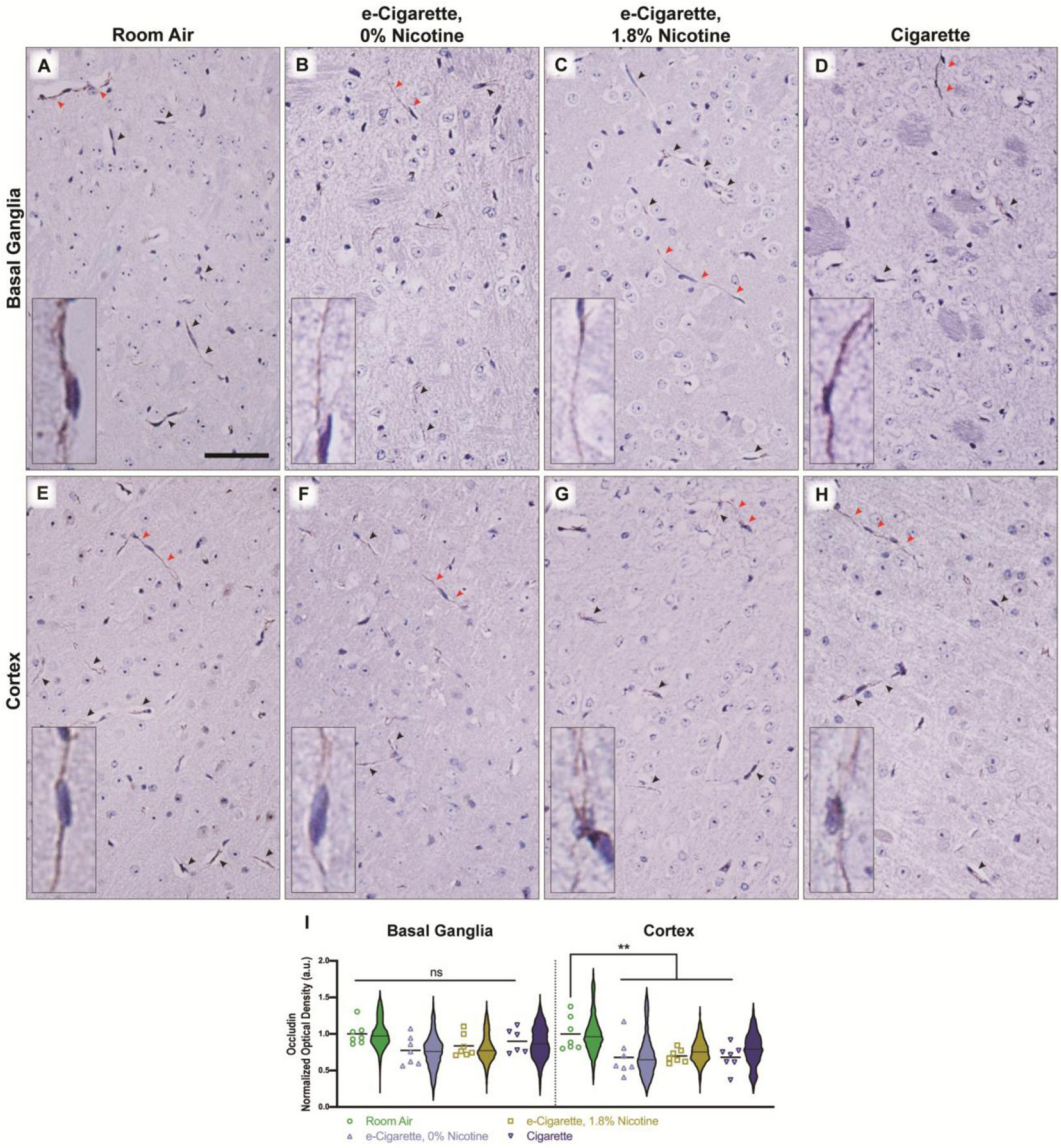


**Figure 4.**

Localization of Occludin is disrupted in vessel tight junctions of the cortex following exposure to e-cigarettes or cigarettes. Whole tissue scans were captured from rostral coronal sections, and separated by region for analysis. Representative images from basal ganglia (A-D) and cortex (E-H) are shown for each treatment group and Occludin-positive microvessels are indicated by arrowheads. Red arrowheads indicate vessels which are shown in the high-magnification inset. Occludin-positive areas were identified by thresholding of red-to-blue ratio value across each brain region of interest, and densitometry values of Occludin-positive area (I) were quantified and normalized to the whole region for basal ganglia and cortex. Mean densitometry of all vessels per animal is shown by individual points (n = 6–7 mice/group) with cross-bar indicating mean of all animals. Violin plots depict the distribution of densitometry for all detected vessels within a treatment group (n = 2465–4839 vessels/group). Statistics were carried out using only individual animal means. **, $p < 0.01$; ns, no

significance versus room air. Two-way ANOVA was applied [exposure, $F(3,47)=6.310$, $p=0.0011$; region, $F(1,47)=0.0249$, $p=0.0249$); interaction, $F(3,47)=0.8543$, $p=0.4714$]. Scale bar, 25 μm.

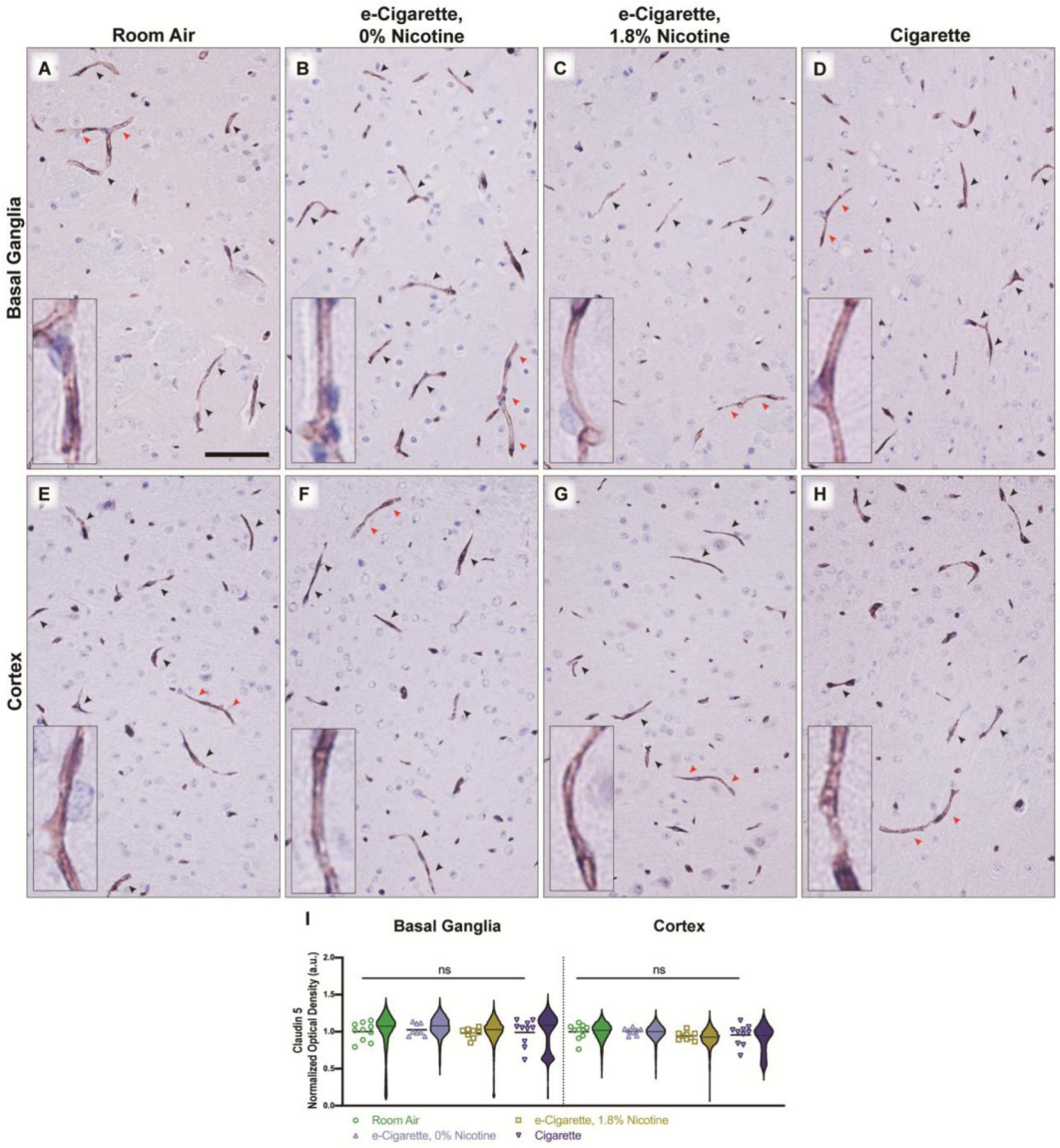


**Figure 5.**

Claudin 5 expression and localization is unaltered by e-cigarettes and cigarettes. Representative images in the basal ganglia (A-D) and cortex (E-H) are shown for each treatment group and Claudin 5-positive microvessels are indicated by arrowheads. Red arrowheads indicate vessels which are shown in the high-magnification inset. Densitometry of all vessels were quantified (I) and the average per animal is shown by individual points (n = 8–10 mice/group), with cross-bar indicating mean of all animals. Violin plots depict distribution of densitometry for all detected vessels within a treatment group (n = 7016–21,682 vessels/group). Statistics were carried out using only individual animal means. ns, no significance versus room air. Two-way ANOVA was applied [exposure, $F(3,65)=0.8489$, $p=0.4722$; region, $F(1,65)=0.7972$, $p=0.3752$]. Scale bar, 25 μm.

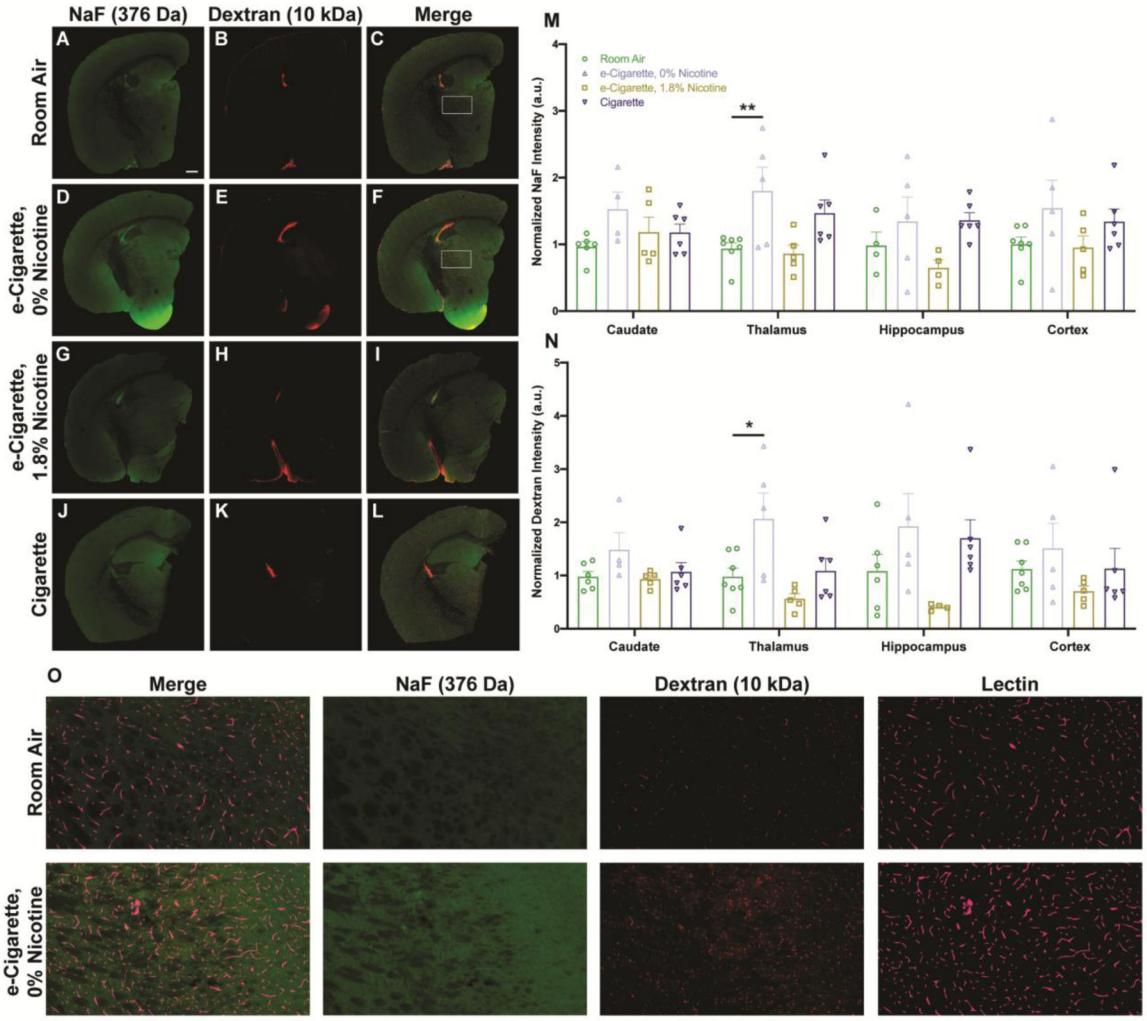


**Figure 6.**

BBB permeability is increased within thalamic nuclei following exposure to nicotine-free e-cigarette products. NaF (green, A, D, G, J) and TMR-dextran (red, B, E, H, K) tracers for permeability were added to the vascular space shortly before tissue harvest along with *Lycopersicon esculentum* lectin (LEL) (cyan, O) as a vascular label. Fresh frozen sections were collected to contain the hippocampus, caudate nucleus, thalamus, and parietal cortex. Merged images of both tracers with LEL are shown (C, F, I, L) with boxed regions of room air and EC0% groups (C, F) shown at higher magnification (O). Fluorescent intensity of NaF (M) and TMR-dextran (N) were quantified for individual regions and normalized to fluorescent intensity of respective tracers in serum. Values for each animal are shown as individual points (n = 4–6 mice/group) with group mean and standard error indicated by bars. *, $p < 0.05$; **, $p < 0.01$ versus room air. Two-way ANOVAs were applied to NaF [exposure, $F(3,70)=8.008$, $p=0.0001$; region, $F(3,70)=0.5105$, $p=0.6763$; interaction, $F(9,70)=0.5623$, $p=0.8232$] and TMR-dextran [exposure, $F(3,72)=8.376$, $p<0.0001$; region, $F(3,72)=0.2591$, $p=0.8546$; interaction, $F(9,72)=0.7451$, $p=0.6665$]. Scale bar, 500 μm.

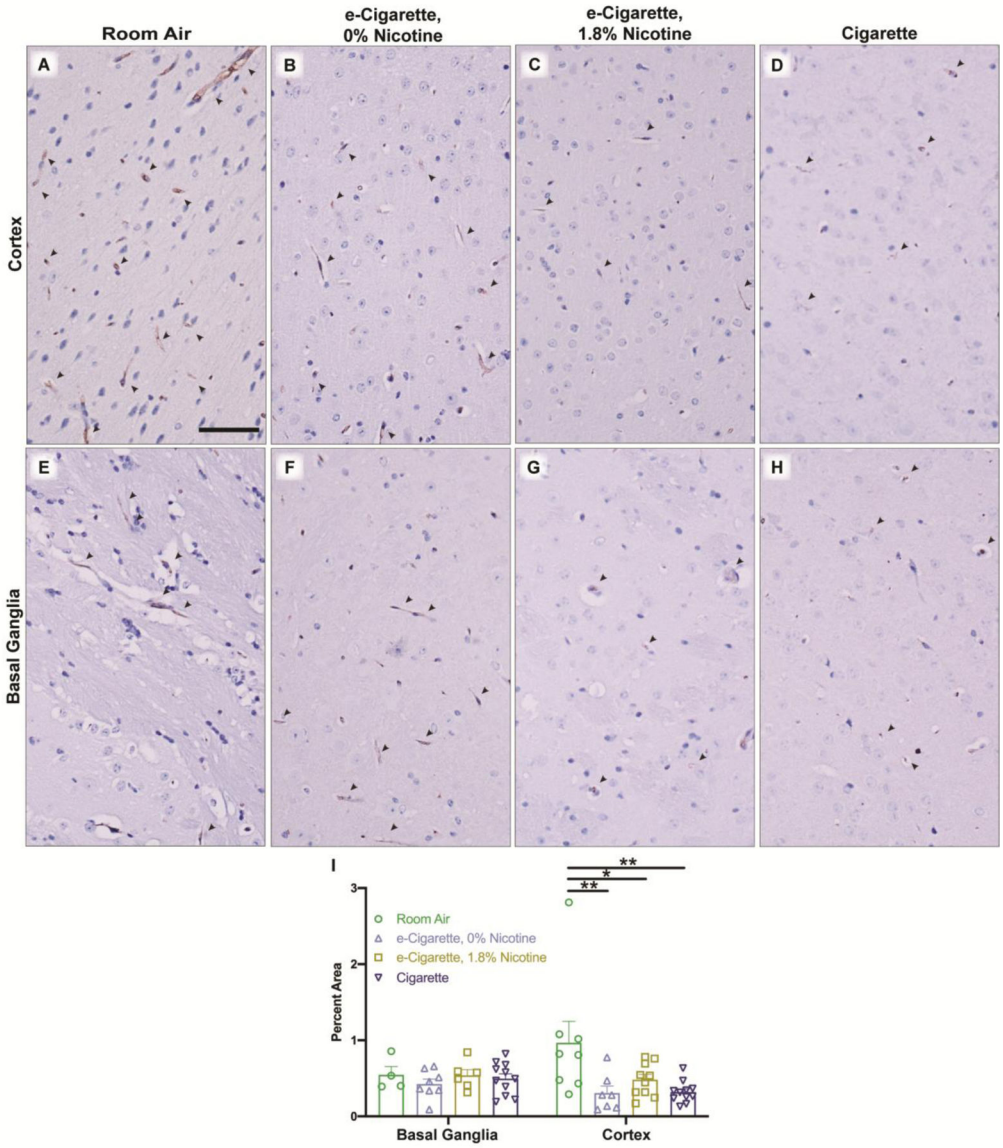


**Figure 7.**

Expression of Glut1 is reduced within cortical microvessels of mice exposed to e-cigarettes or cigarettes. Representative images from whole tissue scans were taken for each treatment group within the frontal cortex (A-D) and basal ganglia (E-H). Arrowheads indicate Glut1 immunoreactivity in vessels with red arrowheads indicating those shown in the high-magnification inset. Glut1-positive areas were identified using red-to-blue ratio of the image and expression was quantified (I) as a percentage of the region of interest which was Glut1 positive. Values for each animal are shown as individual points (n = 4–11 mice/group) with group mean and standard error indicated by bars. *, $p < 0.05$; **, $p < 0.01$ versus room air. Two-way ANOVA was applied [exposure, $F(3,57)=3.374$, $p=0.0244$; region, $F(1,57)=0.0407$, $p=0.8407$; interaction, $F(3,57)=2.049$, $p=0.1172$]. Scale bar, 25 μm.

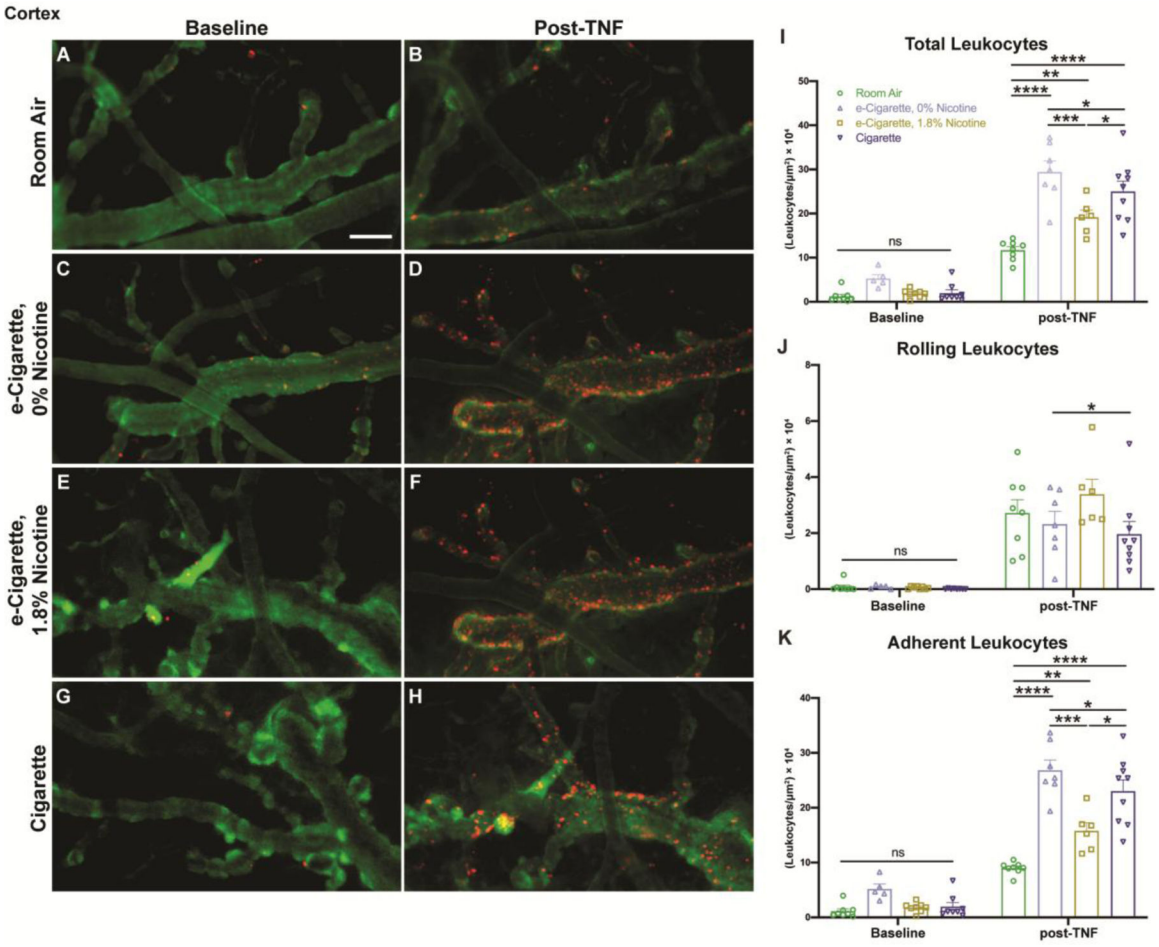


**Figure 8.**

TNF-induced leukocyte adhesion is exacerbated by exposure to e-cigarettes or cigarettes and is of greatest magnitude in the absence of nicotine. Intravital videos of pial microvessels were taken following daily exposure and repeated at 2 hours post-Tnf administration. Representative images show rhodamine 6G labeled leukocytes (red) within dextran-70 kDa-labeled (green) vessels at baseline (A, C, E, G) and following Tnf (B, D, F, H). The total number of leukocytes were quantified and normalized to visible vessel area (I), then further subdivided into rolling (J) and adherent (K) leukocytes based on displacement throughout the video. Individual points represent the mean of 2–3 videos taken per animal (n = 6–8 mice/group) with group mean and standard error indicated by bars. *, $p < 0.05$; **, $p < 0.01$; ***, $p < 0.001$; ****, $p < 0.0001$. Two-way ANOVAs were applied to total [exposure, $F(3,51)=17.99$, $p<0.0001$; timepoint (baseline vs. post-TNF), $F(1,51)=306.0$, $p<0.0001$; interaction, $F(3,51)=8.980$, $p<0.0001$], rolling [exposure, $F(3,51)=1.674$, $p=0.1842$; timepoint, $F(1,51)=106.8$, $p<0.0001$; interaction, $F(3,51)=1.508$, $p=0.2237$], and adherent leukocytes [exposure, $F(3,51)=26.96$, $p<0.0001$; timepoint, $F(1,51)=321.6$, $p<0.0001$; interaction, $F(3,51)=13.90$, $p<0.0001$]. Scale bar, 50 μm.

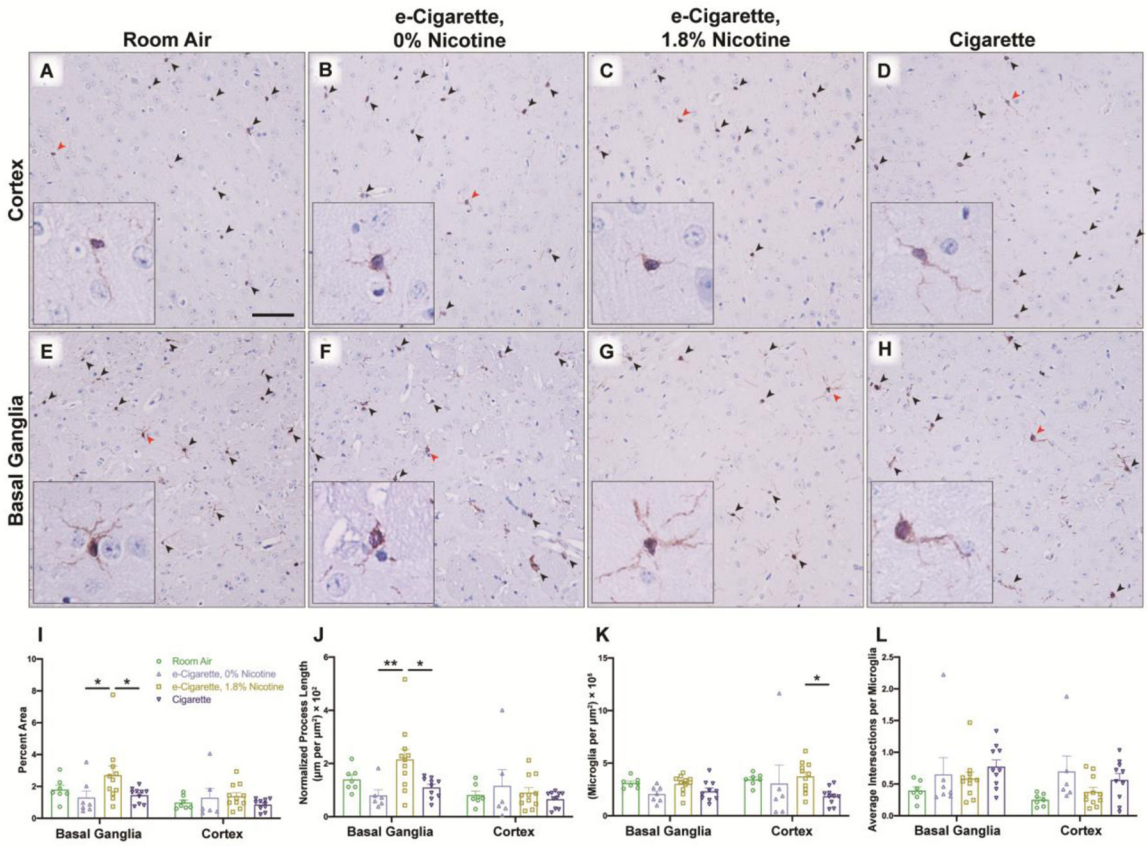


**Figure 9.**

Microglial arborization increases following exposure to nicotine-containing e-cigarettes. Immunoreactivity for Iba1 was assessed in coronal slices containing the frontal cortex (A-D) and basal ganglia (E-H) for each treatment group. Arrowheads denote microglia within representative images, with red arrowheads indicating microglia shown in high-magnification inset. Representations of microglia were constructed from red-to-blue ratio of the image and morphology was analyzed (I-L) by several metrics. Percentage of Iba1-positive area (I), normalized length of visible processes (J), and density of microglial cells (K) was determined for each region. Microglia with cell bodies visible in the plane of section were further assessed (L) for average number of intersection points. Individual points represent values for each animal (n = 7–11 mice/group) with group mean and standard error indicated by bars. *, $p < 0.05$; **, $p < 0.01$. Two-way ANOVAs were applied to Iba1-positive area [exposure, $F(3,61)=2.911$, $p=0.0415$; region, $F(1,61)=6.994$, $p=0.0104$; interaction, $F(3,61)=1.117$, $p=0.3494$], length [exposure, $F(3,60)=2.744$, $p=0.0508$;region, $F(1,60)=6.135$, $p=0.0161$; interaction, $F(3,60)=2.889$, $p=0.0428$], cell density [exposure, $F(3,61)=3.118$, $p=0.0325$; region, $F(1,61)=1.086$, $p=0.3014$; interaction, $F(3,61)=0.8063$, $p=0.4953$], and intersection points [exposure, $F(3,61)=3.112$, $p=0.0327$; region, (1,61)=1.980, $p=0.1645$; interaction, $F(3,61)=0.3871$, $p=0.7627$]. Scale bar, 25 μm.

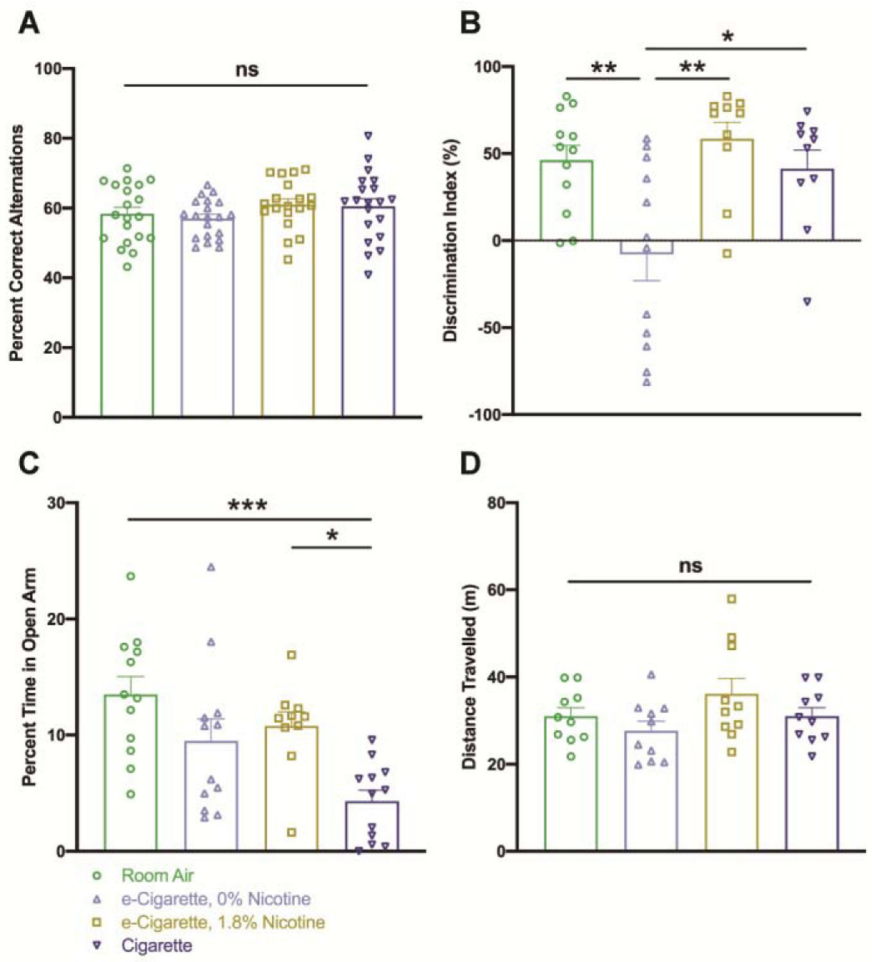


**Figure 10.**

Recognition memory within the novel object recognition paradigm is impaired following exposure to nicotine-free e-cigarettes. Mice were tested for cognitive and affective alternations by several measures at 3 hours following the daily exposure period. Cognition was assessed by Y-maze spontaneous alternation task (A) and novel object recognition paradigm (B). Percentage of correct alternations (A) denotes the proportion of three-entry fragments within the sequence of arm entries that contain all three arms. Discrimination index (DI) denotes the difference in time spent exploring the novel versus familiar object as a percentage of total time spent exploring. Anxiety-related behavior was investigated by elevated plus maze (C) and changes in locomotor activity were controlled for by quantifying total distance travelled within the open-field paradigm (D). Values for each animal are shown by individual points (n = 19–20 for Y-maze, n = 8–12 for all other tests) with group mean and standard error indicated by bars. *, $p < 0.05$; **, $p < 0.01$; ***, $p < 0.001$. One-way ANOVAs were applied to Y-maze [$F(3,75)=1.087$, $p=0.3601$], NORT [$F(3,40)=6.754$, $p=0.0009$], EPM [$F(3,42)=7.069$, $p=0.0006$], and open field [$F(3,36)=1.940$, $p=0.1405$].